



# RESEARCH MEMORANDUM

THE LONGITUDINAL STABILITY AND CONTROL CHARACTERISTICS OF  
A 60° DELTA-WING MISSILE HAVING HALF-DELTA TIP CONTROLS  
AS OBTAINED FROM A FREE-FLIGHT INVESTIGATION AT  
TRANSONIC AND SUPERSONIC SPEEDS

By Martin T. Moul and Hal T. Baber, Jr.

Langley Aeronautical Laboratory  
Langley Field, Va.

**NATIONAL ADVISORY COMMITTEE  
FOR AERONAUTICS**

**WASHINGTON**

October 3, 1952

Declassified August 28, 1956

NATIONAL ADVISORY COMMITTEE FOR AERONAUTICS

RESEARCH MEMORANDUM

THE LONGITUDINAL STABILITY AND CONTROL CHARACTERISTICS OF  
A 60° DELTA-WING MISSILE HAVING HALF-DELTA TIP CONTROLS  
AS OBTAINED FROM A FREE-FLIGHT INVESTIGATION AT  
TRANSONIC AND SUPERSONIC SPEEDS

By Martin T. Moul and Hal T. Baber, Jr.

SUMMARY

A rocket-propelled model of a cruciform 60° delta-wing missile configuration having half-delta tip controls has been flight-tested in the Mach number range 0.70 to 1.65. Longitudinal stability derivatives, control effectiveness, and drag characteristics were obtained by use of the square-wave pulsed-control technique.

The lift curves were smooth and linear within the angle-of-attack range ( $\pm 10^\circ$ ) of the test. No unusual trends were noted in the stability derivatives with the exception of the damping-in-pitch derivative which, contrary to theory, had a minimum value at a Mach number of 1.31. The lift-curve slope at supersonic speeds was less than the modified slender-body theory results by from 7 to 9 percent. The aerodynamic center shifted rearward 8-percent mean aerodynamic chord at transonic speeds. Pitching effectiveness of the tip controls was maintained through the Mach number range but was reduced at supersonic speeds to about one-half the subsonic value. The steady-state angle of attack per unit control deflection at supersonic speeds was only 44 percent of the subsonic value.

INTRODUCTION

One type of control surface proposed for use on triangular wings at supersonic speeds is the half-delta tip control. Such a control on a 60° sweptback delta wing (ref. 1) has provided satisfactory rolling effectiveness and indicated good possibilities for aerodynamic balancing. Additional control-force and hinge-moment characteristics for a number of hinge-axis locations have been reported in reference 2. In order to

provide longitudinal-control data, an investigation of a cruciform missile having triangular wings and tip control surfaces was undertaken.

From the flight test of a missile configuration having  $60^\circ$  delta wings and half-delta tip control surfaces, the longitudinal stability, control, and drag characteristics for a Mach number range of 0.70 to 1.65 are presented. The results are compared with those of a  $60^\circ$  delta-wing airplane configuration having constant-chord full-span controls and with theory.

#### SYMBOLS

c	wing chord, ft
$\bar{c}$	wing mean aerodynamic chord, ft
S	total wing area in one plane including body intercept, sq ft
t	wing thickness, inches; or time, seconds
W	weight, pounds
$I_y$	moment of inertia about Y-axis, slug-ft <sup>2</sup>
g	acceleration due to gravity, ft/sec <sup>2</sup>
$\alpha$	angle of attack, deg
$\delta$	control deflection, deg
$a_n/g$	normal accelerometer reading, g units
$a_l/g$	longitudinal accelerometer reading, g units
$a_t/g$	transverse accelerometer reading, g units
V	velocity of model, ft/sec
$V_c$	speed of sound in air, ft/sec
M	Mach number, $V/V_c$
$\rho$	mass density of air, slugs/cu ft
$\mu$	coefficient of viscosity, slugs/ft-sec

R	Reynolds number, $\rho V \bar{c} / \mu$
q	dynamic pressure, lb/sq ft; or pitching velocity, radians/sec
P	period, sec
b	exponential damping coefficient in $e^{-bt}$ , per sec
$C_L$	lift coefficient, $\left( \frac{a_n}{g} \cos \alpha + \frac{a_l}{g} \sin \alpha \right) \frac{W}{qS}$
$C_D$	drag coefficient, $\left( -\frac{a_l}{g} \cos \alpha + \frac{a_n}{g} \sin \alpha \right) \frac{W}{qS}$
$C_m$	pitching-moment coefficient, $\frac{\text{Pitching moment about center of gravity}}{qS\bar{c}}$
$C_{L\text{trim}}$	trim lift coefficient
$\alpha_{\text{trim}}$	trim angle of attack, deg
$C_{D\text{min}}$	minimum drag coefficient
$(L/D)_{\text{max}}$	maximum lift-drag ratio
$dC_D/dC_L^2$	drag due to lift
$\alpha/\delta$	amplitude ratio
$\phi$	phase angle, deg
$\omega$	angular forcing frequency, radians/sec
$\dot{\alpha}$	$\frac{1}{57.3} \frac{d\alpha}{dt}$ , radians/sec

Derivatives:

$$C_{L\alpha} = \frac{\partial C_L}{\partial \alpha}, \text{ per deg;}$$

$$C_{L\delta} = \frac{\partial C_L}{\partial \delta}, \text{ per deg}$$

$$C_{m\alpha} = \frac{\partial C_m}{\partial \alpha}, \text{ per deg;}$$

$$C_{m\delta} = \frac{\partial C_m}{\partial \delta}, \text{ per deg}$$

$$C_{mq} = \frac{\partial C_m}{\partial \frac{q\bar{c}}{2V}}, \text{ per rad;}$$

$$C_{m\dot{\alpha}} = \frac{\partial C_m}{\partial \frac{\dot{\alpha}\bar{c}}{2V}}, \text{ per rad}$$

## MODEL AND APPARATUS

### Model Description

A sketch of the model arrangement is presented in figure 1. The body consisted of a 7-inch-diameter cylindrical section and ogival nose and tail cones and had an over-all fineness ratio of 13.1. Triangular wings were mounted on the body in a cruciform arrangement.

Wing and tip-control detail are presented in figure 2. The solid magnesium wings had a modified hexagonal airfoil section of constant thickness; the plan form was triangular, the leading edge being swept back  $59^{\circ} 32'$ . The tips of two opposite wing panels were replaced by steel, all-movable, half-delta, control surfaces mounted on steel torque rods. The controls had a double-wedge section and a constant thickness ratio of 3 percent. There was a parting-line gap between the control and wing of 0.03 inch. The ratio of exposed wing area (inclusive of controls) to control area was 9:1. Photographs of the model and the wing-control arrangement are presented in figure 3.

A hydraulic pulsing system supplied from an accumulator was utilized to provide a programmed square-wave deflection of the controls. The two control deflections were  $\pm 9.6^{\circ}$ . At a Mach number of about 1.0, the pulse frequency was decreased by means of a switch, sensitive to total-head pressure, which decreased the voltage field of the programming motor.

The model was boosted to supersonic velocities by means of a solid-propellant rocket motor of 6000-pound thrust and 3-second duration. The launching technique was the same as that reported in reference 3.

The physical characteristics of the model are presented in the following table:

Weight and balance:	
Weight, lb . . . . .	87.4
Center of gravity, percent $\bar{c}$ back of leading edge of $\bar{c}$ . . . . .	12.6
$I_y$ , slug-ft <sup>2</sup> . . . . .	8.1
Wing:	
Total wing area in one plane, sq ft . . . . .	2.84
Mean aerodynamic chord, ft . . . . .	1.46
Thickness ratio at wing-body juncture . . . . .	0.03
Tip control:	
Area in one plane, sq ft . . . . .	0.19
Mean aerodynamic chord, ft . . . . .	0.38

#### INSTRUMENTATION

The model was equipped with an NACA 8-channel telemeter which transmitted continuous records of normal (2 ranges), longitudinal, and transverse accelerations, angle of attack, control deflection, total pressure, and a calibrated static pressure. Angle of attack was measured by a free-floating vane extended from the nose on a sting and total pressure by a total-pressure tube extended below the body. The positions of these two instruments are shown in figure 1.

The model trajectory was determined by a modified SCR-584 type radar tracking unit. Model velocity was obtained from a CW Doppler velocimeter and from total and static pressures. A radiosonde released at the time of flight measured temperatures and atmospheric pressures through the altitude range traversed by the model.

#### TECHNIQUE

As the model decelerated through the Mach number range, longitudinal responses were produced by a programmed square-wave deflection of the tip controls. The angle of attack measured at the nose was corrected to the center of gravity by the methods of reference 4. The normal acceleration and corrected angle-of-attack oscillations were analyzed by the methods of reference 3 to determine the stability and control derivatives.

When the model drag was analyzed, the lift range at supersonic speeds was not large enough to yield experimental values of maximum lift-drag ratio. At these Mach numbers calculated values of  $(L/D)_{\max}$  were obtained from

$$\frac{1}{\sqrt{4(C_{D\min})\left(\frac{dC_D}{dC_L^2}\right)}}$$

which assumes the extensions of the lift-drag polars to vary as a parabola.

Although the model encountered transverse accelerations up to  $\pm 2.5g$  during the flight, no effects of yaw were noted on the longitudinal responses.

#### ACCURACY

The measured quantities are believed to be accurate within the following limits:

M	Limit of accuracy of				
	M	$\alpha$	$\delta$	$C_L$	$C_{D\min}$
0.8	$\pm 0.07$	$\pm 0.4$	$\pm 0.2$	$\pm 0.019$	$\pm 0.010$
1.6	$\pm 0.03$	$\pm 0.4$	$\pm 0.2$	$\pm 0.004$	$\pm 0.002$

These errors, dependent upon telemeter and radar precision, are primarily systematic in nature; parameters which are dependent upon differences in measured quantities, such as  $C_{L\alpha}$  and  $\Delta\alpha/\Delta\delta$ , are more accurately determined than the above errors indicate.

## RESULTS AND DISCUSSION

The scale of the flight test is presented in figure 4; Reynolds number, based on wing mean aerodynamic chord, varied from  $5.5 \times 10^6$  to  $16.3 \times 10^6$ . Sample time histories of the model flight at subsonic and supersonic speeds are presented in figure 5. The Mach number variation with time, programmed control deflection, measured angle of attack, normal, and longitudinal accelerations are presented. Differences in pulse duration, model natural frequency, and angle-of-attack range between subsonic and supersonic speeds may be noted.

## Static Stability

Pitching moment.- In figure 6 is presented the variation with Mach number of the period of oscillation. From 0.602 second at  $M = 0.70$  the period decreased to 0.205 second at  $M = 1.63$ .

The static stability derivative  $C_{m\alpha}$  was reduced from the period of oscillation and presented in figure 7. A transonic increase in  $C_{m\alpha}$ , of about  $-0.005$ , is noted between Mach numbers 0.90 and 1.00. At supersonic speeds  $C_{m\alpha}$  decreased gradually from  $-0.0136$  at  $M = 1.0$  to  $-0.0083$  at  $M = 1.63$ .

Lift.- From lift-coefficient and angle-of-attack time histories, lift-curve plots were constructed for determining lift-curve slope  $C_{L\alpha}$ . Some typical plots are presented in figure 8 for control deflections of  $\pm 9.6^\circ$ . The lift curves are smooth and linear within the angle-of-attack range of this test.

The slopes of the lift curves were measured and are presented in figure 9. Lift-curve slope increased from 0.0438 at  $M = 0.72$  to a peak value of 0.0525 at  $M = 1.02$ . As the Mach number continued to increase,  $C_{L\alpha}$  decreased to 0.0387 at  $M = 1.62$ .

At a Mach number of 1.62 a comparison is made with unpublished data from tests conducted in the Langley 9-inch supersonic tunnel of a similar wing-body configuration differing in body length. The wind-tunnel configuration was longer by a scaled 25-inch cylindrical section inserted between the wing and the nose. Good agreement is shown in the  $C_{L\alpha}$  of these models.

The lift-curve slope of a  $60^\circ$  delta-wing airplane reported in reference 5 is presented for comparison. Comparable body-upwash effects

are expected for the airplane and the missile since the body-diameter—wing-span ratios were nearly equal, being 0.226 for the airplane and 0.219 for the missile. The lift-curve slopes agreed favorably at supersonic speeds, but a difference is noted at transonic speeds. This difference is attributable to the critical Mach numbers, the airplane having a lower critical Mach number because of its 65-series airfoil, 6.5-percent-thick section.

In reference 6 Nielsen and Kaattari have modified the slender-body-theory results for lift-curve slopes of wing-body combinations having cylindrical afterbodies. From figure 9, theory is seen to predict the lift-curve-slope trend, with the test values being 7 to 9 percent lower than the theoretical values at all Mach numbers. This difference is believed attributable to the basic-wing experimental lift-curve slope being less than theory (for example, ref. 7) rather than to any negative lift realized by the tail cone.

Aerodynamic center.— The aerodynamic-center location in percent of  $\bar{c}$  is presented in figure 10. Aerodynamic center was at 31 percent  $\bar{c}$  at subsonic speeds and shifted rearward in the transonic range to 39 percent  $\bar{c}$  at  $M = 1.05$ . With further increasing Mach number, the aerodynamic center shifted gradually forward. The transonic aerodynamic-center shift was only 8 percent  $\bar{c}$  for this configuration as compared to 12 percent  $\bar{c}$  for the canard configuration of reference 3. In reference 7 the aerodynamic center of a wing-body combination having a cylindrical afterbody is determined from modified slender-body theory. Good agreement is shown between this test and theory and indicates that the loss of lift on the tail cone is slight as suggested in the lift discussion. Also presented are the aerodynamic-center locations for a delta-wing airplane having a shorter forebody (ref. 5) and a delta-wing missile having a longer forebody. As expected, the configuration with the shortest forebody had the most rearward aerodynamic-center location. The change in missile forebody length caused an aerodynamic-center movement of 15 percent  $\bar{c}$  as compared with a predicted movement of 10 percent  $\bar{c}$  from the modified slender-body theory.

### Dynamic Stability

The exponential damping constant  $b$  is determined from the amplitude ratios of the decaying oscillations by the methods of reference 3 and is presented as a function of Mach number in figure 11. The exponential damping constant varied from 1.10 at  $M = 0.70$  to 3.0 at  $M = 1.55$  with a slight decrease occurring between  $M = 1.10$  and 1.30.

The damping-in-pitch derivative  $C_{m_q} + C_{m_{\dot{\alpha}}}$  is shown in figure 12. The trend of  $C_{m_q} + C_{m_{\dot{\alpha}}}$  with Mach number with minimum points occurring

at Mach numbers 0.97 and 1.33, is unusual. With increasing Mach number above 1.33  $C_{m_q} + C_{m\dot{\alpha}}$  increases rapidly to a maximum value of -3.33 at a Mach number of 1.62. The trend through the Mach number range 0.75 to 1.10 is similar to that of the canard missile of reference 3 in that the minimum and maximum points occur in the same order. Modified slender-body-theory results of reference 8 for a delta-wing-body configuration with no afterbody predict approximate magnitudes but do not predict the Mach number trend. The damping-in-pitch derivative of a  $60^\circ$  delta-wing airplane configuration (ref. 5) is seen to be greater than the missile damping through most of the supersonic Mach number range. From a consideration of center-of-gravity locations (20.7 percent  $\bar{c}$  for airplane and 12.6 percent  $\bar{c}$  for missile) and body lengths, a greater damping-in-pitch derivative would have been predicted for the missile than for the airplane. The accuracy of  $C_{m_q} + C_{m\dot{\alpha}}$  is questionable since the lift and damping-in-pitch terms which contribute to the total damping (ref. 3) are approximately equal in magnitude. Any error occurring in  $C_{L\alpha}$  or  $b$  will cause a correspondingly larger error in  $C_{m_q} + C_{m\dot{\alpha}}$ .

It should be noted that although the damping-in-pitch derivative of wing-body combinations may be extremely small compared with that of some present-day wing-tail missile configurations, the differences in total damping are not so great. For example, a comparison of the tailless model of this paper with the canard missile configuration of reference 3 shows that, although the ratio of damping-in-pitch derivatives is 10:1, the ratio of total damping is about 3:1.

#### Control Effectiveness

Longitudinal trim curves.— The trim angles of attack are presented in figure 13 for the two programmed control deflections. For the control deflection of  $-9.6^\circ$ ,  $\alpha_{trim}$  decreases from  $4^\circ$  at  $M = 0.7$  to  $2.1^\circ$  at  $M = 1.15$  and then increases to  $2.6^\circ$  at  $M = 1.60$ . The larger trim angles of attack at subsonic speeds result from the smaller static stability at these speeds. The differences in  $\alpha_{trim}$  for the two equal control deflections indicate an out-of-trim condition which is possibly due to slight asymmetries in the model and in the angle-of-attack indicator.

In figure 14 is presented the trim-lift coefficients for the two control deflections. The  $C_{Ltrim}$  curves resemble the  $\alpha_{trim}$  curves, the values decreasing with increasing Mach number. There is an out-of-trim lift coefficient as there was an out-of-trim angle of attack.

The trim lift per trim angle of attack of this configuration is about 30 percent less than that of the canard configuration because of the negative  $C_{m\delta}$  of the tip controls.

Trim angle of attack and lift per unit control deflection.- From the  $\alpha_{\text{trim}}$  curves the trim angle of attack per unit control deflection is determined and presented as a function of Mach number in figure 15. The  $\Delta\alpha_{\text{trim}}/\Delta\delta$  decreases abruptly near a Mach number of 1.0 and, at supersonic speeds, is only 44 percent of the subsonic value.

The change in trim-lift coefficient due to a unit control deflection is presented in figure 16. From 0.0166 at  $M = 0.7$ , the value of  $\Delta C_{L_{\text{trim}}}/\Delta\delta$  decreases rapidly to 0.0065 at  $M = 1.40$  primarily because of the rearward aerodynamic-center shift at transonic speeds.

Control lift and pitching effectiveness.- The control lift effectiveness  $C_{L\delta}$  including the lift induced on the wing was determined from the trim conditions of angle of attack and lift coefficient as in reference 3 and is presented in figure 17. From 0.0039 at  $M = 0.70$ ,  $C_{L\delta}$  increases with Mach number to a peak of 0.0062 at  $M = 0.91$  and then decreases gradually to 0.0022 at  $M = 1.62$ . Lagerstrom (ref. 9) has obtained from the linearized theory the lift of a half-delta tip-control surface on a triangular wing and the corresponding wing-induced lift. The linearized theory does not predict the experimental results although the Mach number trends are similar.

Control-surface pitching effectiveness  $C_{m\delta}$  is presented in figure 18. Pitching effectiveness remains nearly constant at subsonic speeds but decreases gradually at supersonic speeds. At a Mach number of 1.5,  $C_{m\delta}$  is about 56 percent of the subsonic value.

The  $C_{m\delta}$  of a  $60^\circ$  delta-wing airplane having constant-chord, full-span elevons (ref. 5) is also presented, after being corrected to the center-of-gravity location for comparable static stability. The ratio of control area to total wing area for the airplane is 2.46 that of the missile so that a larger  $C_{m\delta}$ , based on total wing area, is expected for the airplane. The ratio of  $C_{m\delta}$  of the airplane to  $C_{m\delta}$  of the missile varies from 3.6 at a Mach number of 0.9 to 2.6 at a Mach number of 1.6 and indicates that the trailing-edge flap is the more effective control. Over the Mach number range, however, the loss of effectiveness is greater for the trailing-edge flap and at  $M = 1.6$  the pitching effectiveness of the two controls is about equal.

## Drag

The variation of total drag of the model with lift coefficient is shown in the drag polars of figure 19 for a Mach number range of 0.75 to 1.55. The subsonic and supersonic polars indicate that the induced drag varied parabolically with the lift; however, this variation was altered slightly in the transonic range due to the rapid increase in wave drag with Mach number.

Minimum drag coefficient as a function of Mach number is shown in figure 20. This is the drag at zero lift of the model with controls at  $9.6^\circ$ . A sharp drag rise occurred at transonic speeds reaching a peak of  $C_{D_{\min}} = 0.055$  at  $M = 1.10$ . The minimum drag coefficient decreased gradually through the supersonic region to a value of 0.043 at  $M = 1.55$ .

The variation of drag due to lift with Mach number is shown in figure 21. A subsonic value of 0.55 was obtained for  $dC_D/dC_L^2$  at  $M = 0.7$ . The trend showed a decrease to 0.43 at  $M = 1.0$  and a slight increase for the tested supersonic range. The same trend was indicated for  $1/57.3C_{L_\alpha}$  with a slightly greater increase at supersonic speeds.

The maximum lift-drag ratio, shown in figure 22, was measured directly from drag polars at subsonic and transonic speeds. At supersonic speeds, the condition of maximum lift-drag ratio was not attained by the model. Calculated values of  $(L/D)_{\max}$  were obtained for these Mach numbers by using  $C_{D_{\min}}$ ,  $dC_D/dC_L^2$ , and by assuming a parabolic variation of drag with lift. The data indicate that  $(L/D)_{\max}$  decreased from 6.3 at  $M = 0.70$  to 3.2 at  $M = 1.1$  and then gradually increased to 3.6 at  $M = 1.55$ .

## Frequency Response

Comparison of the results of two methods for determining longitudinal frequency-response characteristics from transient-response data is made in figure 23 for two Mach numbers. One method employs the experimental stability derivatives and the linearized equations of motion. The second method, as outlined in reference 10, utilizes the Fourier synthesizer to analyze the experimental transient-response data. In the analysis, amplitudes at 24 equal time increments were used to represent the transient response.

For both Mach numbers the resonant frequencies as determined by the two methods are in good agreement and indicate the linearity of the static stability derivative. The peak amplitudes are a function of the

system damping and in figure 23 indicate a difference in damping. From the amplitudes the damping ratios (percent of critical damping) were obtained and were found to be only slightly different for the two methods. For  $M = 1.60$  the damping ratios were 0.11 and 0.13, respectively, for the calculated and synthesizer methods. The same ratios were 0.10 and 0.13 for the  $M = 0.74$  case. At  $M = 1.60$  the phase-angle curves are noted to diverge at higher frequencies. For a linear system of this order, the phase angle should approach  $-180^\circ$  at these frequencies (verified by the calculated results). The trend of the synthesizer phase-angle curve suggests the presence of higher order terms in the transient response or a limitation of the method to a lower frequency range.

### CONCLUSIONS

Results from a flight investigation at Mach numbers 0.70 to 1.65 of a  $60^\circ$  delta-wing missile configuration having half-delta tip controls indicate the following conclusions:

1. No unusual trends were noted in the stability derivatives with the exception of the damping-in-pitch derivative which, contrary to slender-body theory, decreased to a minimum value at a Mach number of 1.33 and then increased with increasing Mach number. The lift curves were smooth and linear within the angle-of-attack range ( $\pm 10^\circ$ ) of the test. The lift-curve slope was in good agreement with that of a tail-less airplane configuration but was less than the modified slender-body-theory results by from 7 to 9 percent. The aerodynamic center was located at 31 percent  $\bar{c}$  at subsonic speeds and shifted rearward 8 percent  $\bar{c}$  at transonic speeds. At supersonic speeds the aerodynamic-center location was in good agreement with modified slender-body-theory results.

2. Pitching effectiveness of the tip controls was maintained through the Mach number range but the value at a Mach number of 1.50 is only 56 percent of the subsonic value. Per unit area the trailing-edge flap was a more effective longitudinal control than the half-delta tip control. The steady-state change in angle of attack per unit control deflection  $\Delta\alpha/\Delta\delta$  at supersonic speeds was only 44 percent of the subsonic value.

3. The minimum drag coefficient was a maximum of 0.055 at a Mach number of 1.10. The variation of drag with lift  $dC_D/dC_L^2$  was larger

than  $1/57.3C_{L\alpha}$  (where  $C_{L\alpha}$  is the lift-curve slope) at all Mach numbers. Maximum lift-drag ratio was 6.3 at subsonic speeds and about 3.4 at supersonic speeds.

Langley Aeronautical Laboratory,  
National Advisory Committee for Aeronautics,  
Langley Field, Va.

1. Martin, G. William, and Church, James D.: Flight Investigation to Determine Force and Hinge-Moment Characteristics at Zero Angle of Attack of a  $60^\circ$  Sweptback Half-Delta Tip Control on a  $60^\circ$  Sweptback Delta Wing at Mach Numbers Between 0.68 and 1.44. NACA RM L5114, 1951.

2. Niewald, Roy J., and Moul, Martin T.: The Longitudinal Stability, Control Effectiveness, and Control Hinge-Moment Characteristics Obtained From a Flight Investigation of a Canard Missile Configuration at Transonic and Supersonic Speeds. NACA RM L5017, 1950.

3. Mitchell, Jesse L., and Peck, Robert F.: An NACA Vane-Type Angle-of-Attack Indicator for Use at Subsonic and Supersonic Speeds. NACA RM L4788, 1949.

4. Micham, Grady L., Grubill, Norman L., and Stevens, Joseph E.: Flight Determination of the Drag and Longitudinal Stability and Control Characteristics of a Rocket-Powered Model of a  $60^\circ$  Delta-Wing Airplane From Mach Numbers of 0.75 to 1.70. NACA RM L5110, 1951.

5. Nielsen, Jack N., and Kattar, George E.: Method for Estimating Lift Interference of Wing-Body Combinations at Supersonic Speeds. NACA RM A5104, 1951.

6. Nielsen, Jack N., Katzen, Elliott D., and Tang, Kenneth K.: Lift and Pitching-Moment Interference Between a Pointed Cylindrical Body and Triangular Wings of Various Aspect Ratios at Mach Numbers of 1.50 and 2.02. NACA RM A5060, 1950.

7. Henderson, Arthur, Jr.: Pitching-Moment Derivatives  $C_{m_p}$  and  $C_{m_q}$  at Supersonic Speeds for a Slender-Delta-Wing and Slender-Body Combination and Approximate Solutions for Broad-Delta-Wing and Slender-Body Combinations. NACA TN 2523, 1951.

8. Lagerstrom, P. A., and Graham, Martha E.: Linearized Theory of Supersonic Control Surfaces. Jour. Aero. Sci., vol. 16, no. 1, Jan. 1949, pp. 31-34.

## REFERENCES

1. Martz, C. William, and Church, James D.: Flight Investigation at Subsonic, Transonic, and Supersonic Velocities of the Hinge-Moment Characteristics, Lateral-Control Effectiveness, and Wing Damping in Roll of a 60° Sweptback Delta Wing With Half-Delta Tip Ailerons. NACA RM L51G18, 1951.
2. Martz, C. William, Church, James D., and Goslee, John W.: Free-Flight Investigation To Determine Force and Hinge-Moment Characteristics at Zero Angle of Attack of a 60° Sweptback Half-Delta Tip Control on a 60° Sweptback Delta Wing at Mach Numbers Between 0.68 and 1.44. NACA RM L51I14, 1951.
3. Niewald, Roy J., and Moul, Martin T.: The Longitudinal Stability, Control Effectiveness, and Control Hinge-Moment Characteristics Obtained From a Flight Investigation of a Canard Missile Configuration at Transonic and Supersonic Speeds. NACA RM L50I27, 1950.
4. Mitchell, Jesse L., and Peck, Robert F.: An NACA Vane-Type Angle-of-Attack Indicator for Use at Subsonic and Supersonic Speeds. NACA RM L9F28a, 1949.
5. Mitcham, Grady L., Crabill, Norman L., and Stevens, Joseph E.: Flight Determination of the Drag and Longitudinal Stability and Control Characteristics of a Rocket-Powered Model of a 60° Delta-Wing Airplane From Mach Numbers of 0.75 to 1.70. NACA RM L51I04, 1951.
6. Nielsen, Jack N., and Kaattari, George E.: Method for Estimating Lift Interference of Wing-Body Combinations at Supersonic Speeds. NACA RM A51J04, 1951.
7. Nielsen, Jack N., Katzen, Elliott D., and Tang, Kenneth K.: Lift and Pitching-Moment Interference Between a Pointed Cylindrical Body and Triangular Wings of Various Aspect Ratios at Mach Numbers of 1.50 and 2.02. NACA RM A50F06, 1950.
8. Henderson, Arthur, Jr.: Pitching-Moment Derivatives  $C_{m_q}$  and  $C_{m\dot{\alpha}}$  at Supersonic Speeds for a Slender-Delta-Wing and Slender-Body Combination and Approximate Solutions for Broad-Delta-Wing and Slender-Body Combinations. NACA TN 2553, 1951.
9. Lagerstrom, P. A., and Graham, Martha E.: Linearized Theory of Supersonic Control Surfaces. Jour. Aero. Sci., vol. 16, no. 1, Jan. 1949, pp. 31-34.

10. Moul, Martin T., and Wineman, Andrew R.: Longitudinal Stability and Control Characteristics From a Flight Investigation of a Cruciform Canard Missile Configuration Having An Exposed Wing-Canard Area Ratio of 16:1. NACA RM L52D24a, 1952.

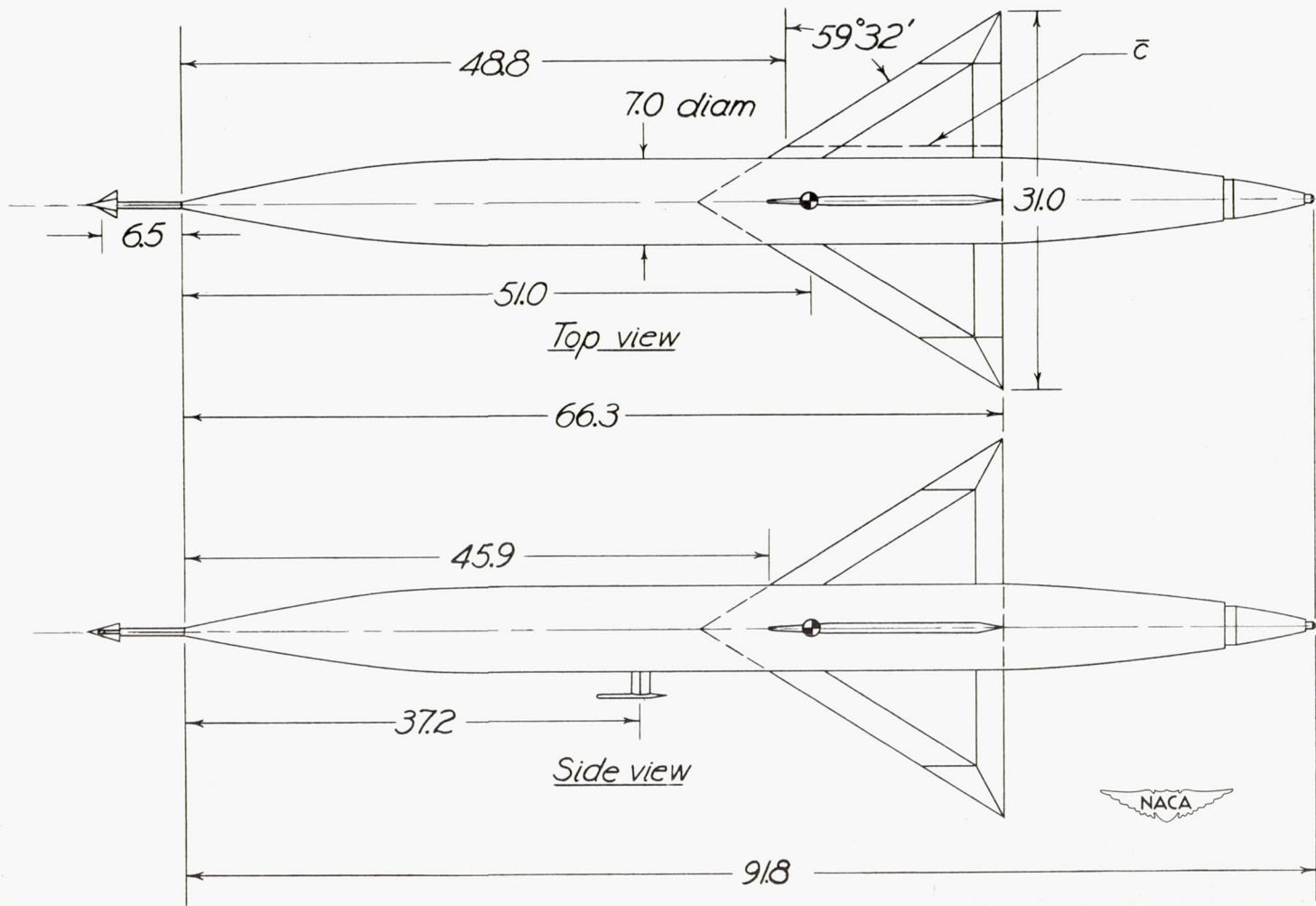


Figure 1.- Model arrangement. All dimensions are in inches.

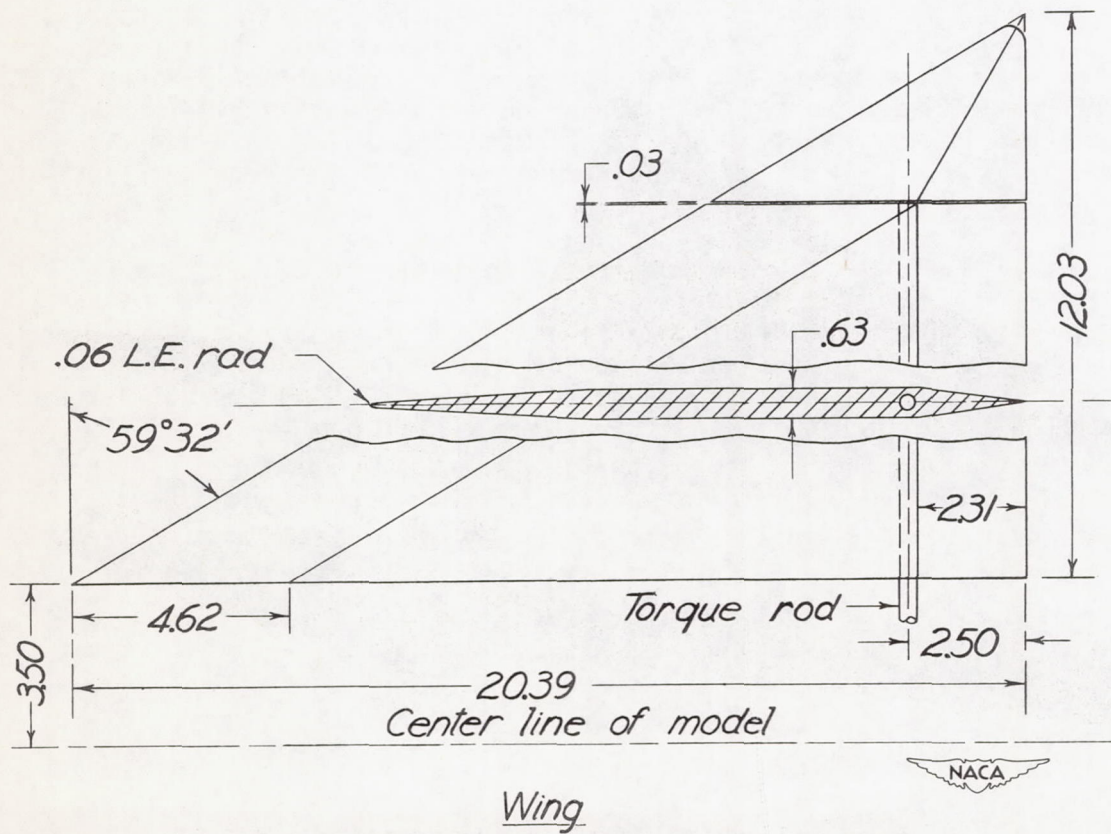
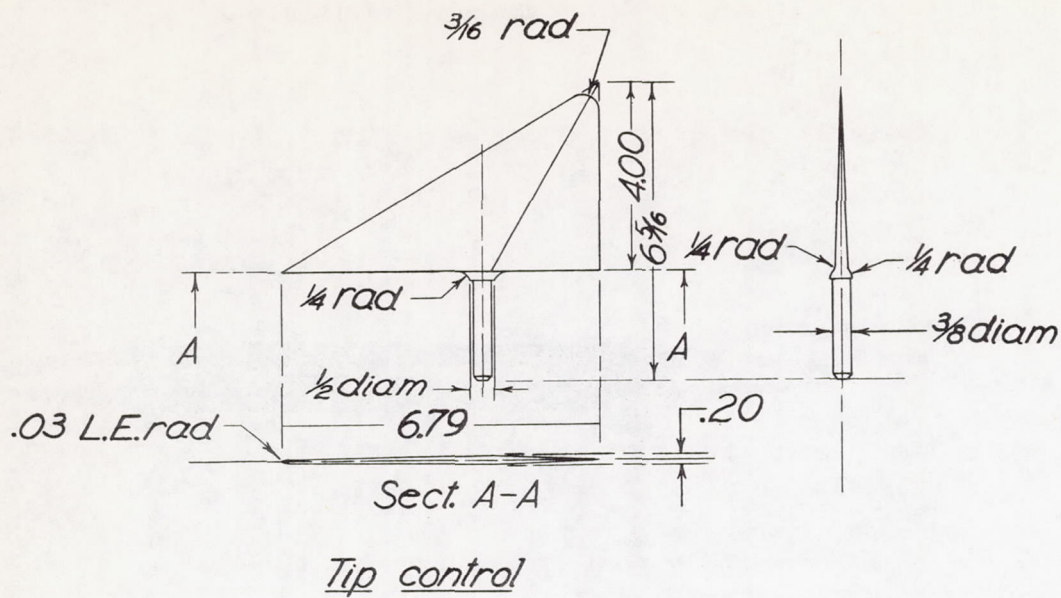
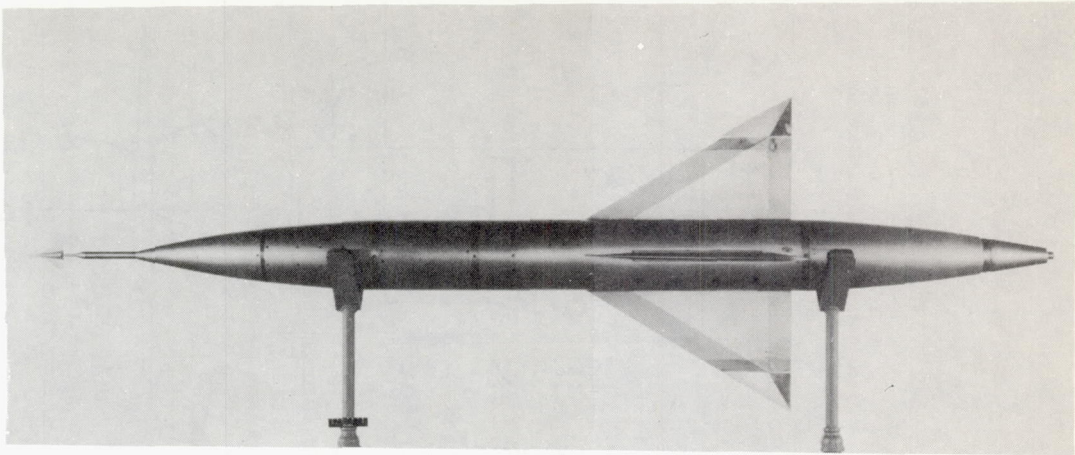
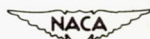
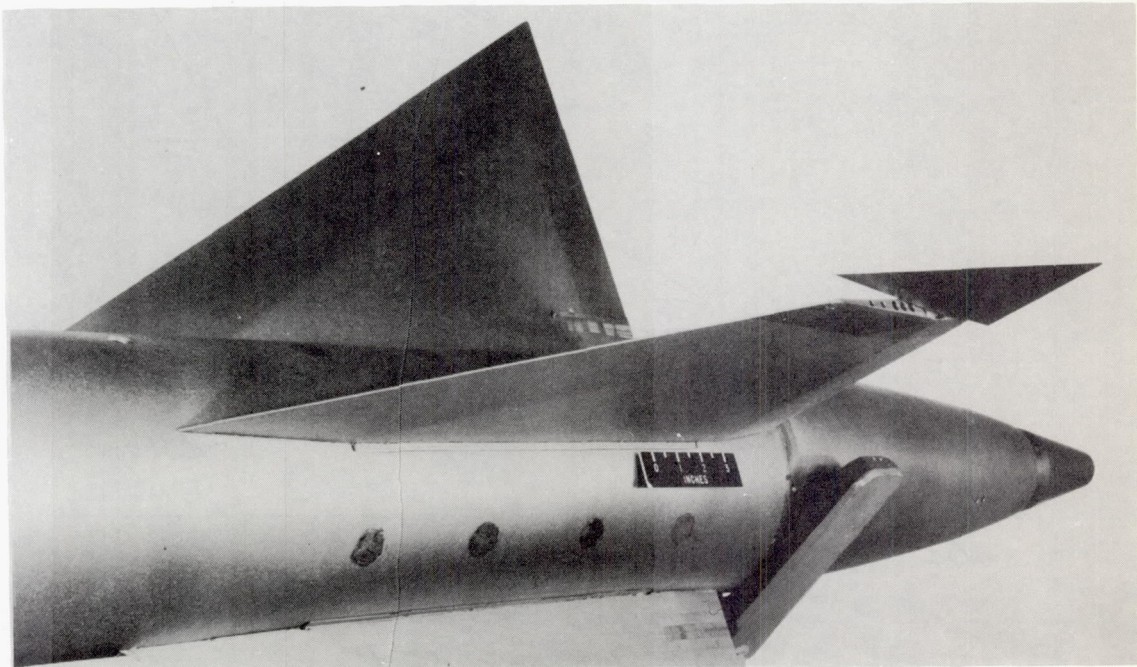


Figure 2.- Wing and tip-control detail. All dimensions are in inches.



(a) Plan view of the model.

  
L-67704.1



(b) Wing and control-surface arrangement.

Figure 3.- Model photographs.

  
L-67706

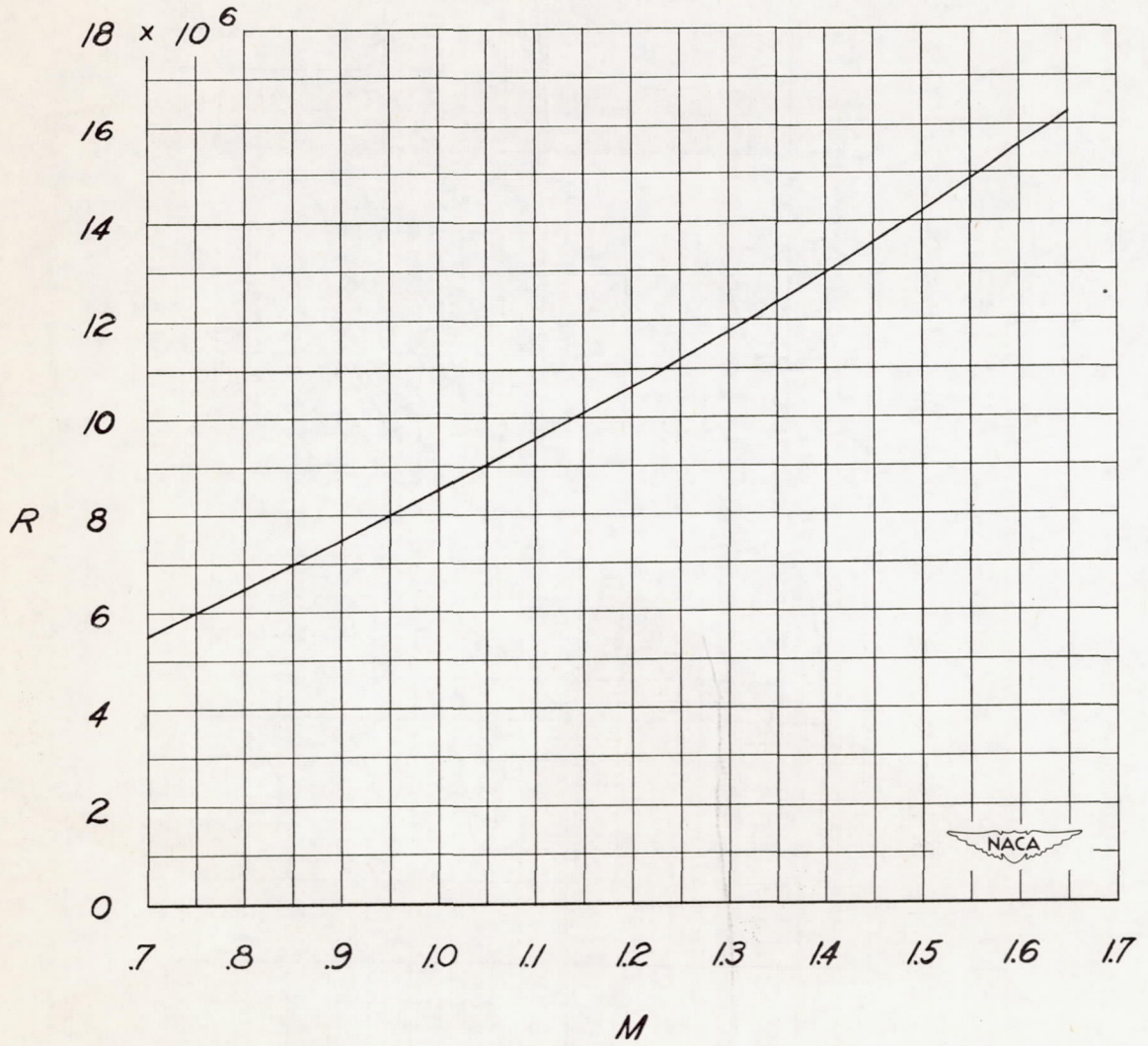
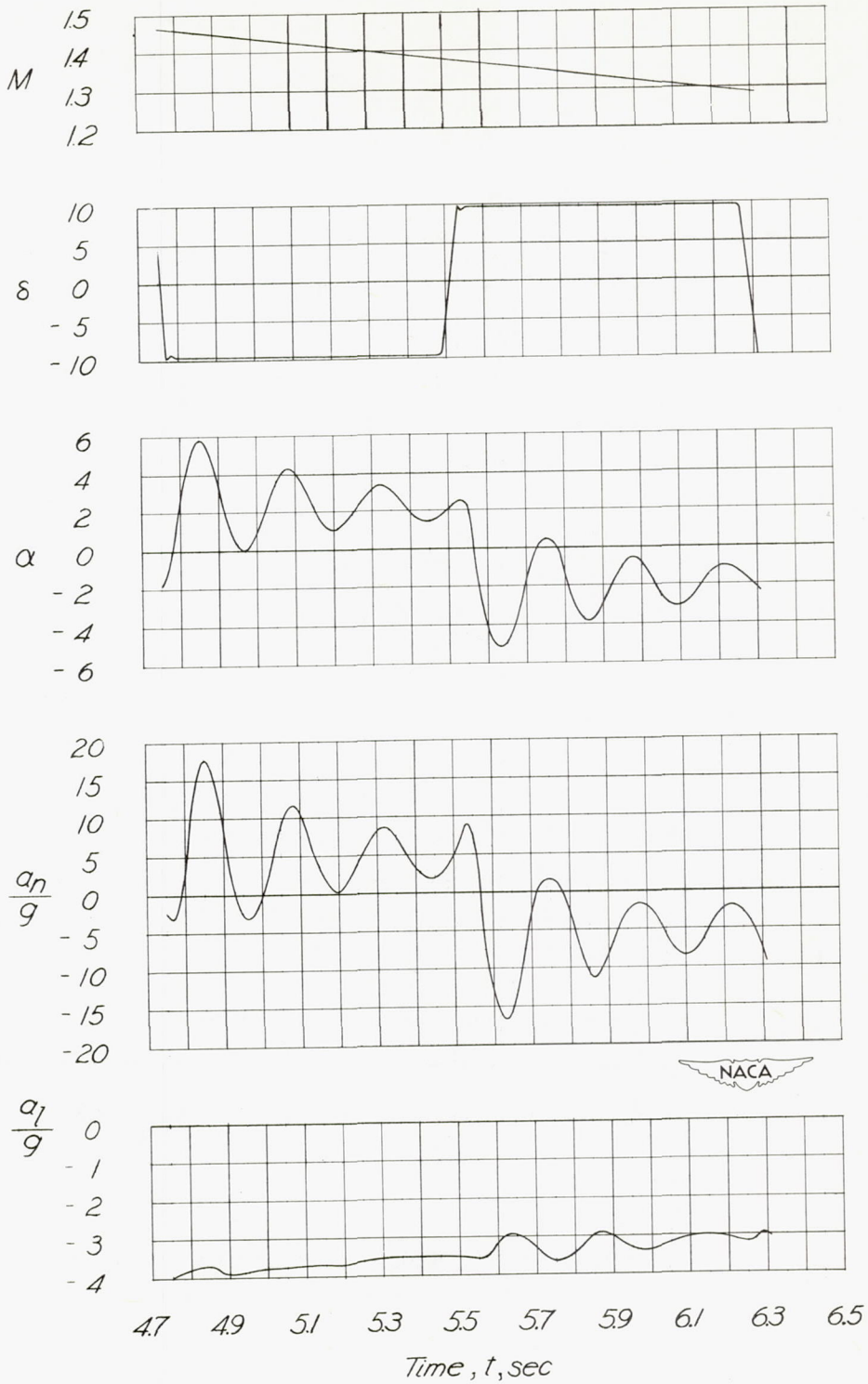
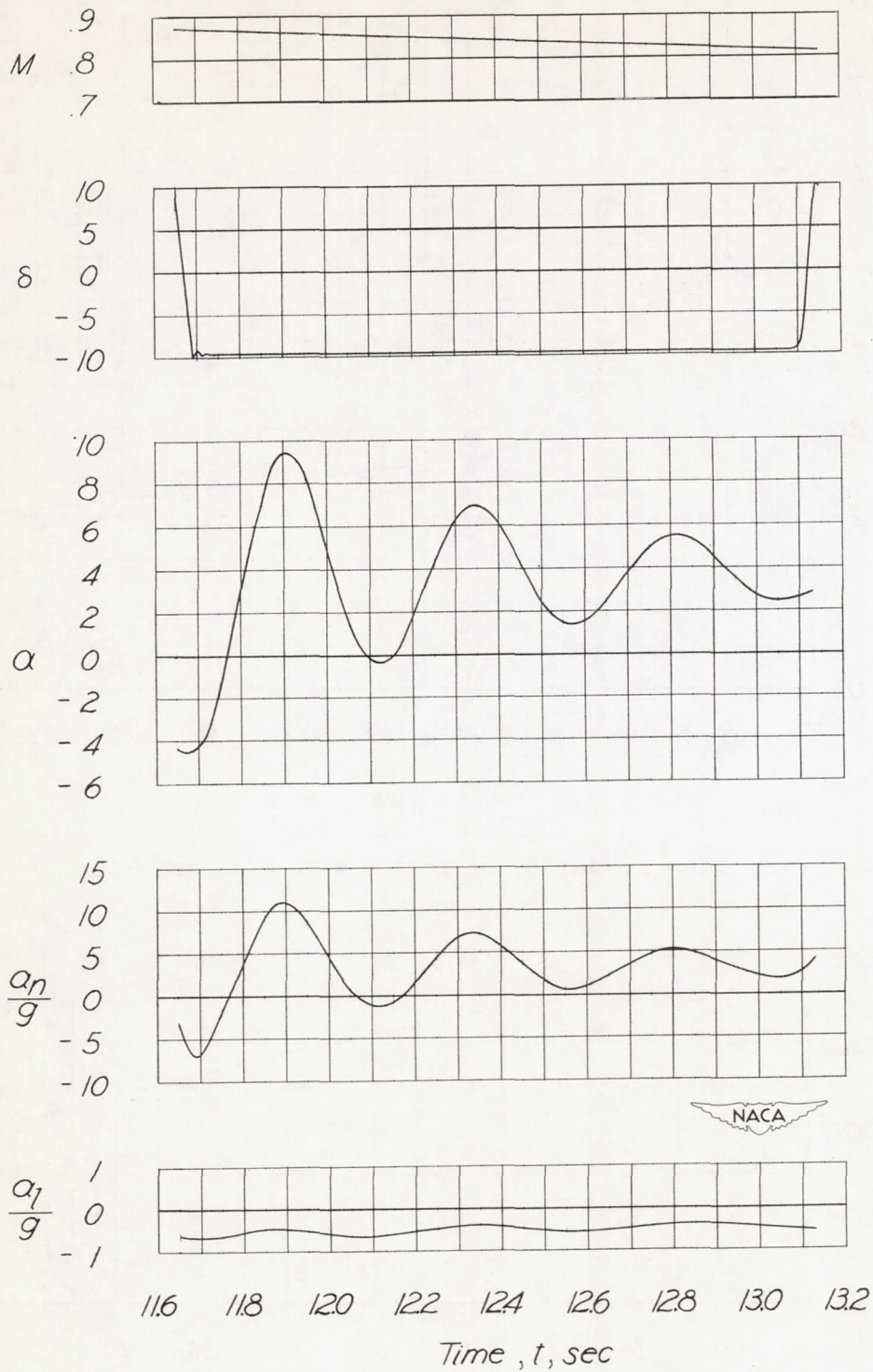


Figure 4.- Scale of flight test, based on wing mean aerodynamic chord of 1.46 feet.



(a) Supersonic.

Figure 5.- Sample time histories of model flight<sup>h+</sup>



(b) Subsonic.

Figure 5.- Concluded.

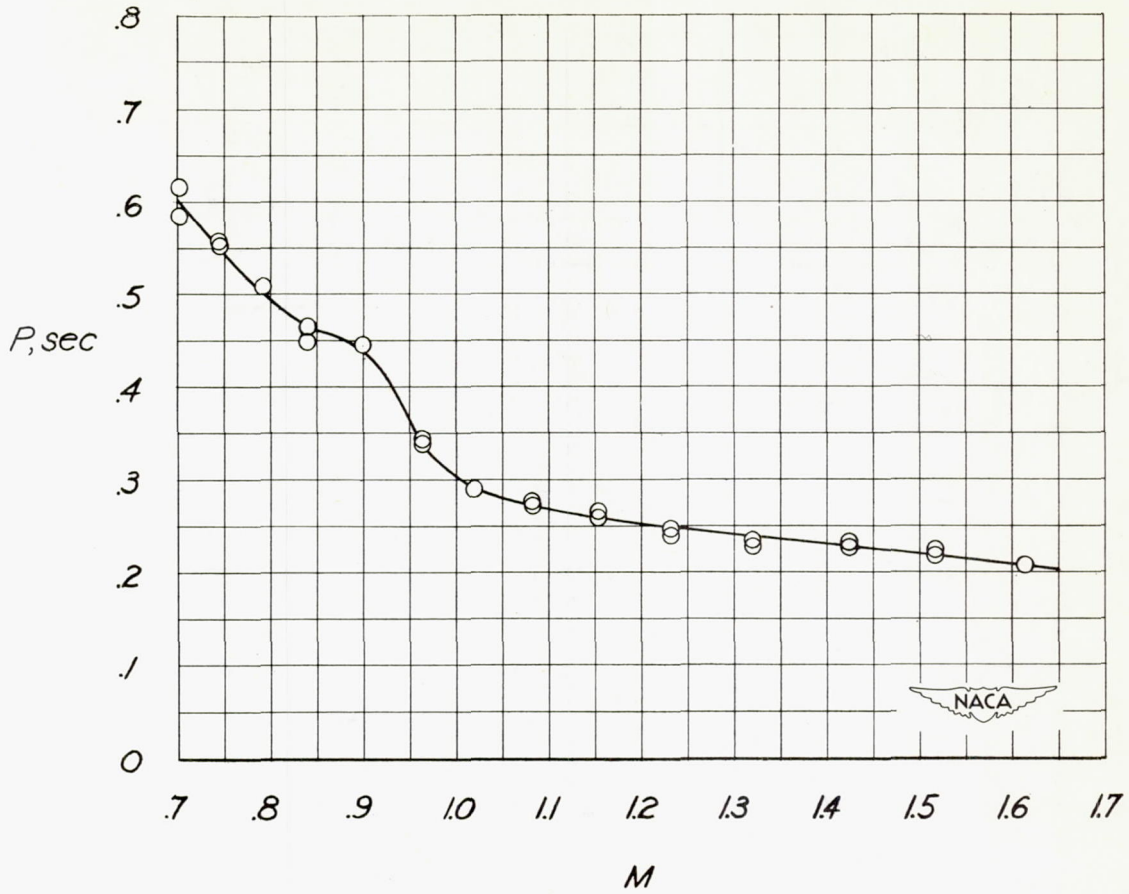


Figure 6.- Variation of period with Mach number.

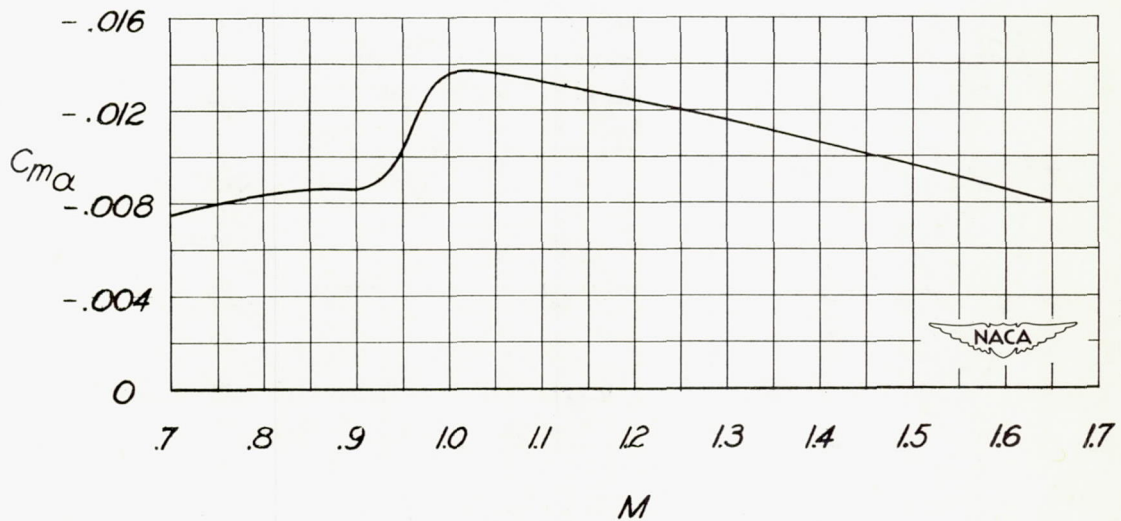
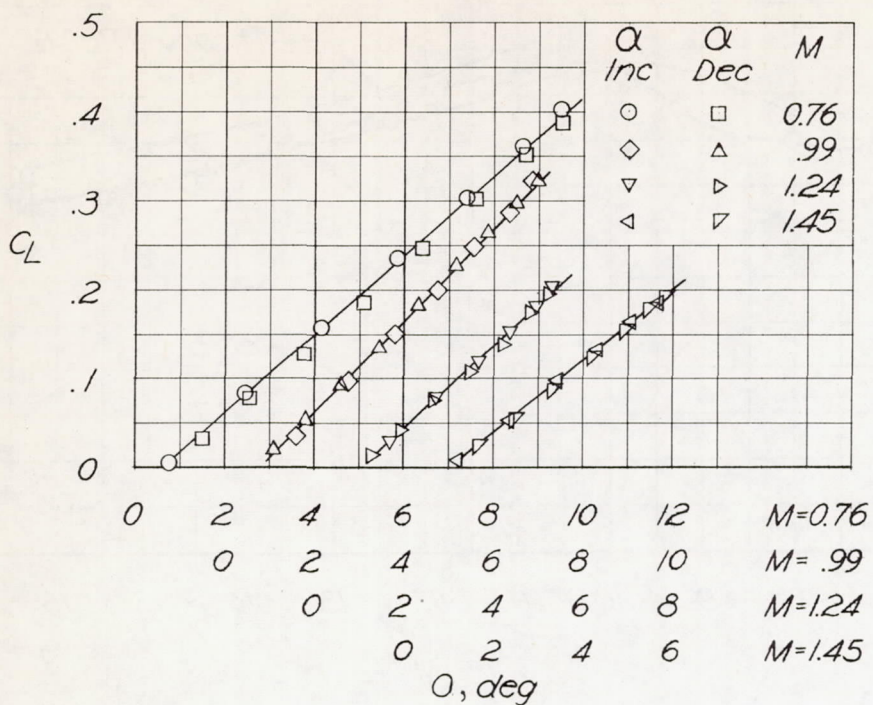
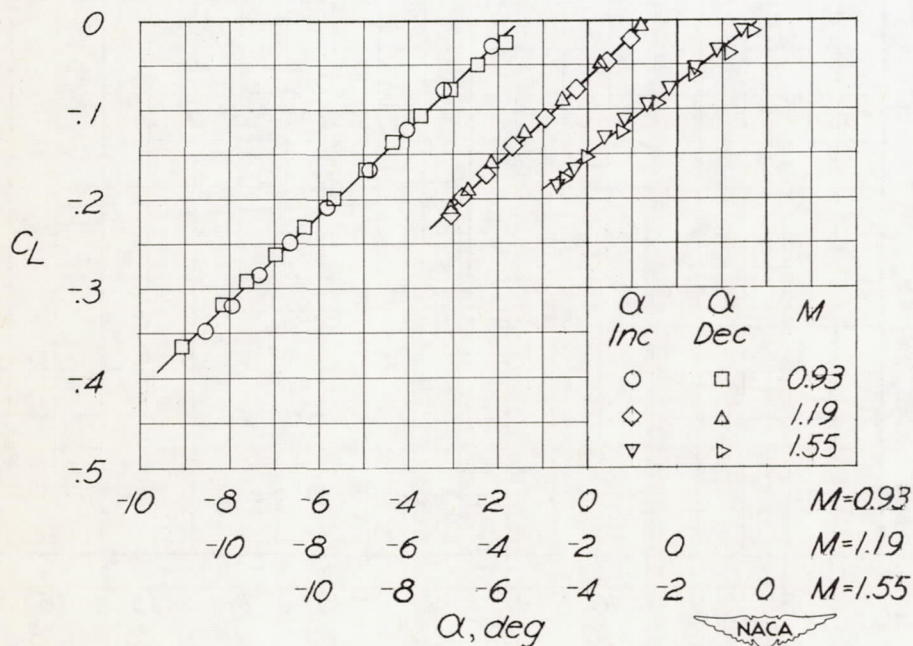


Figure 7.- Variation of static pitching-moment derivative with Mach number.

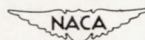


(a)  $\delta = -9.6^\circ$ .



(b)  $\delta = 9.6^\circ$ .

Figure 8.- Typical lift-coefficient variation with angle of attack.



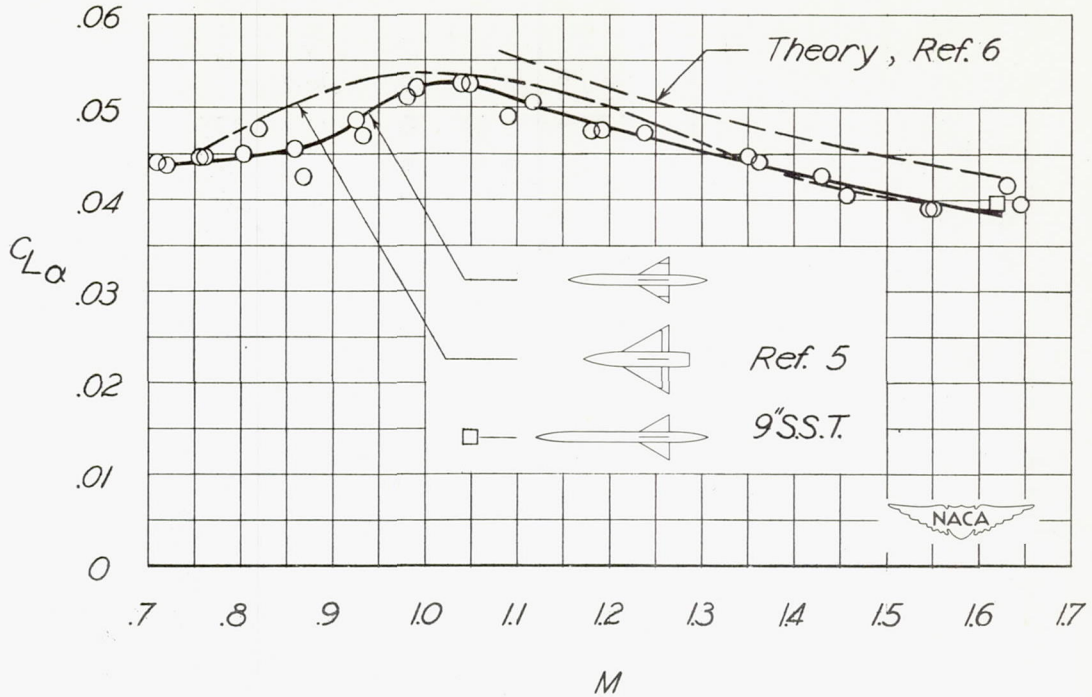


Figure 9.- Variation of lift-curve slope with Mach number.

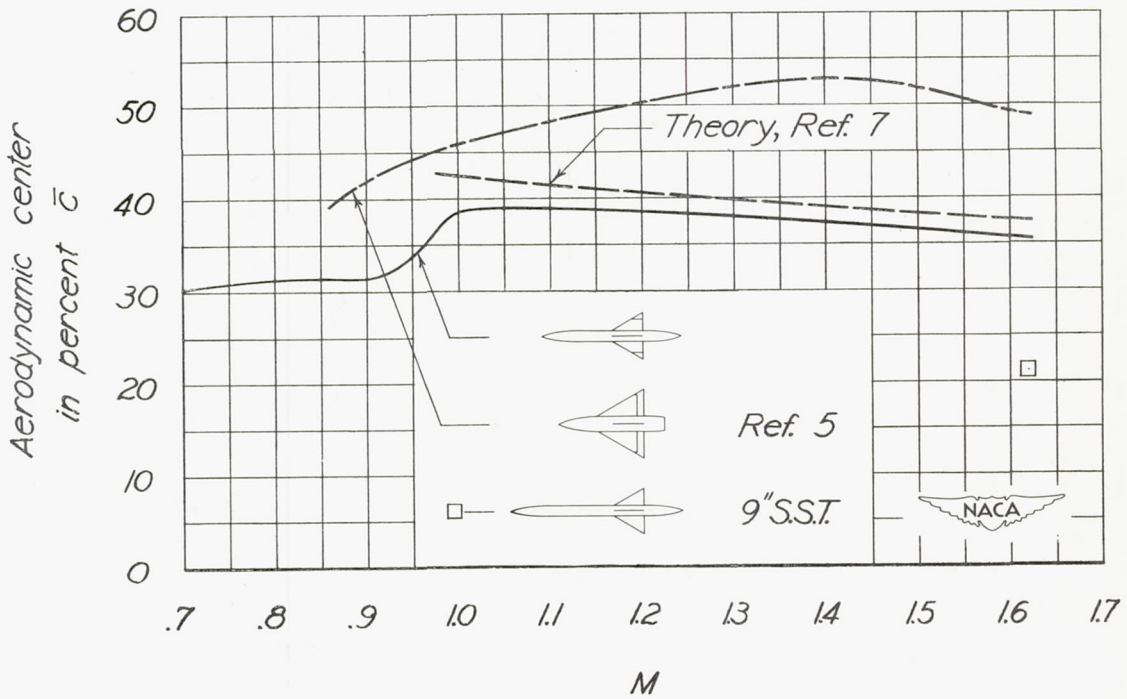


Figure 10.- Variation of aerodynamic-center position with Mach number.

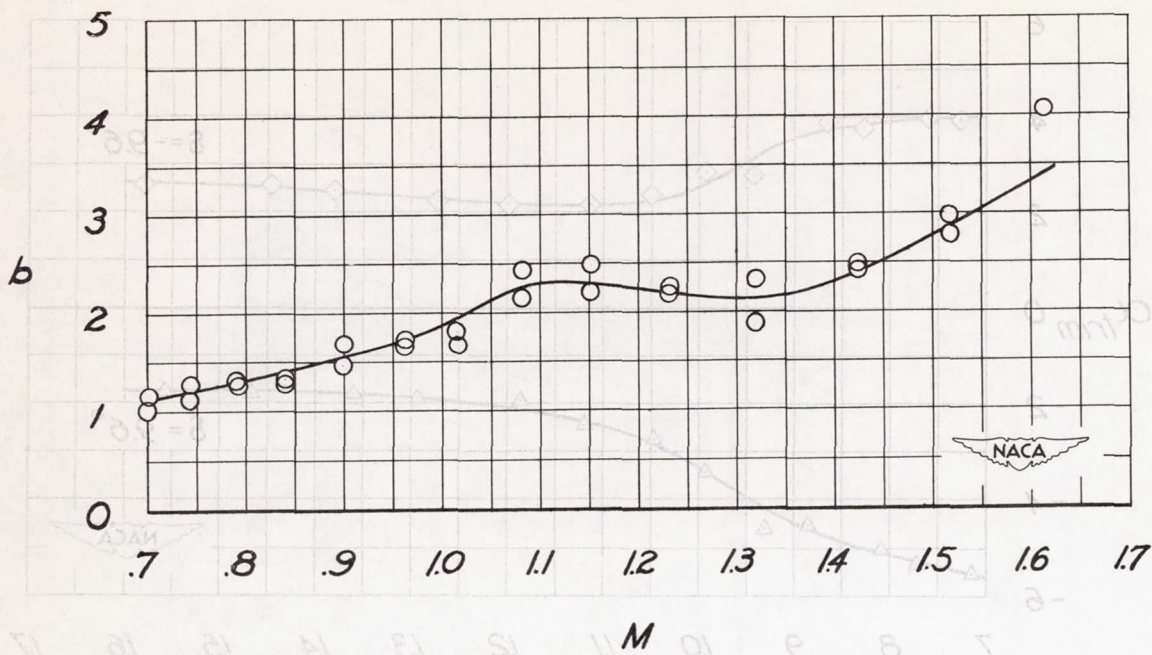


Figure 11.- Variation of exponential damping constant  $b$  with Mach number.

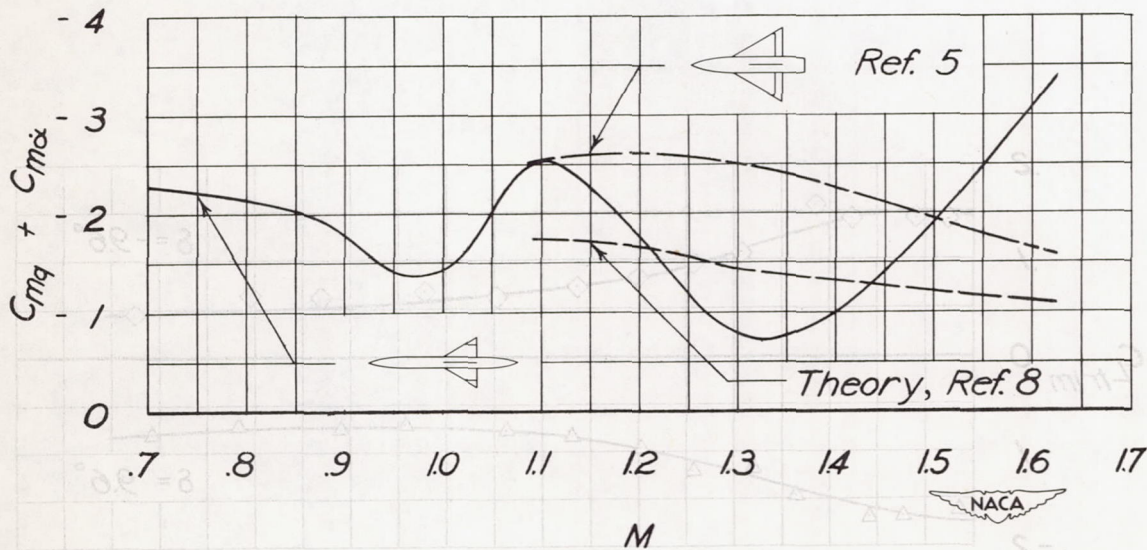


Figure 12.- Variation of aerodynamic damping-in-pitch derivative with Mach number.

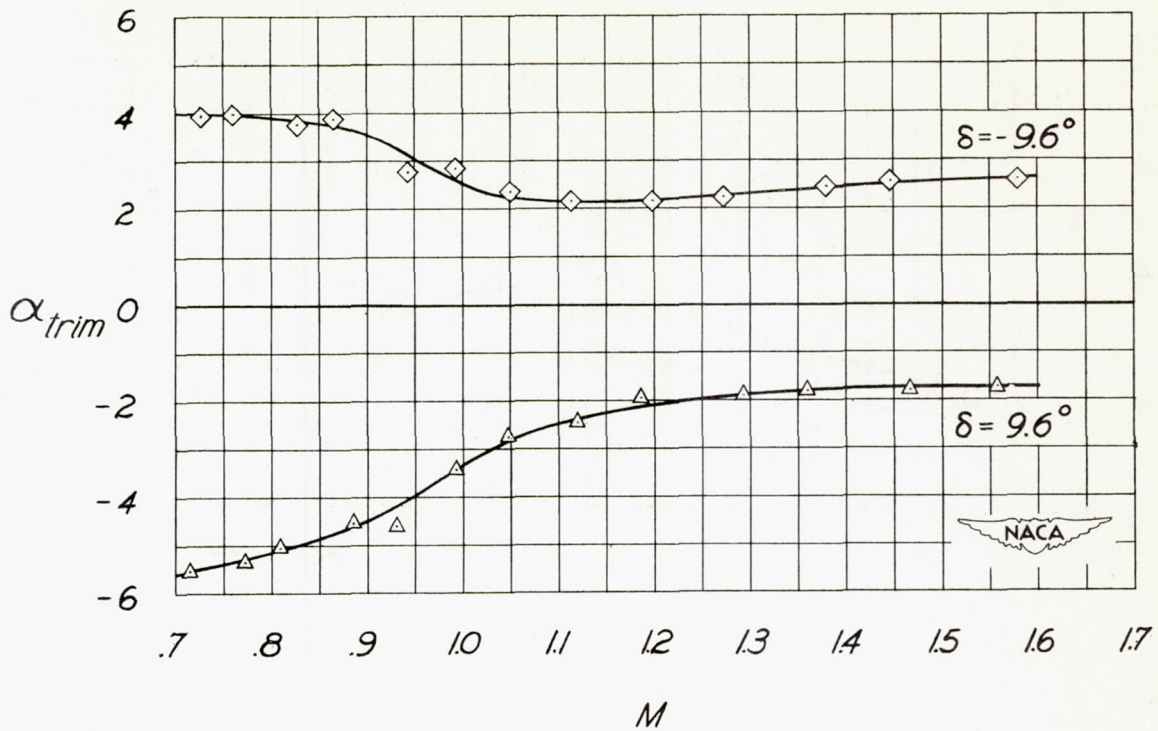


Figure 13.- Variation of trim angle of attack with Mach number.

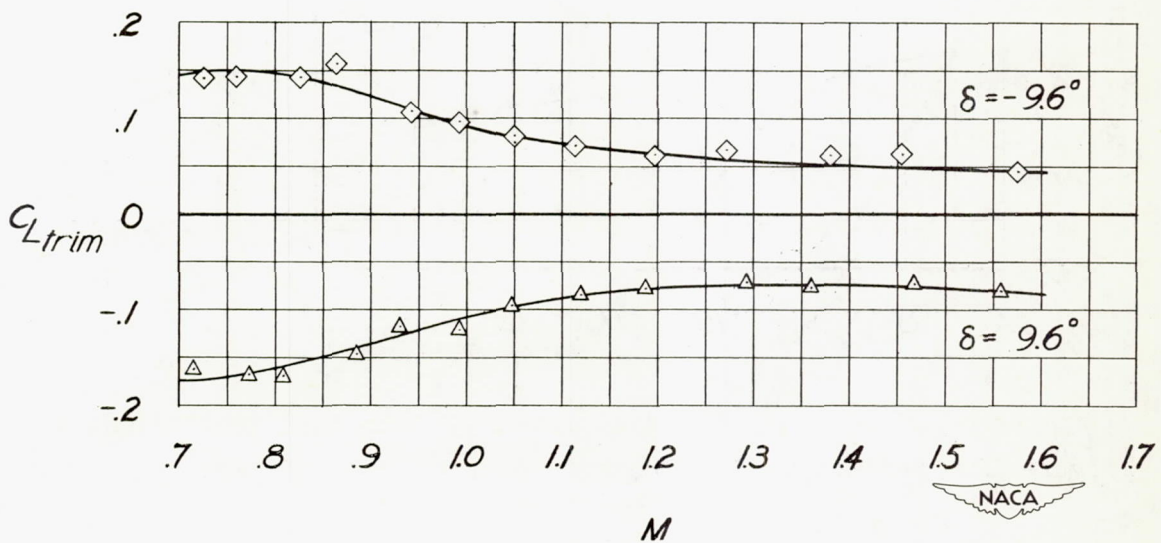


Figure 14.- Variation of trim lift coefficient with Mach number.

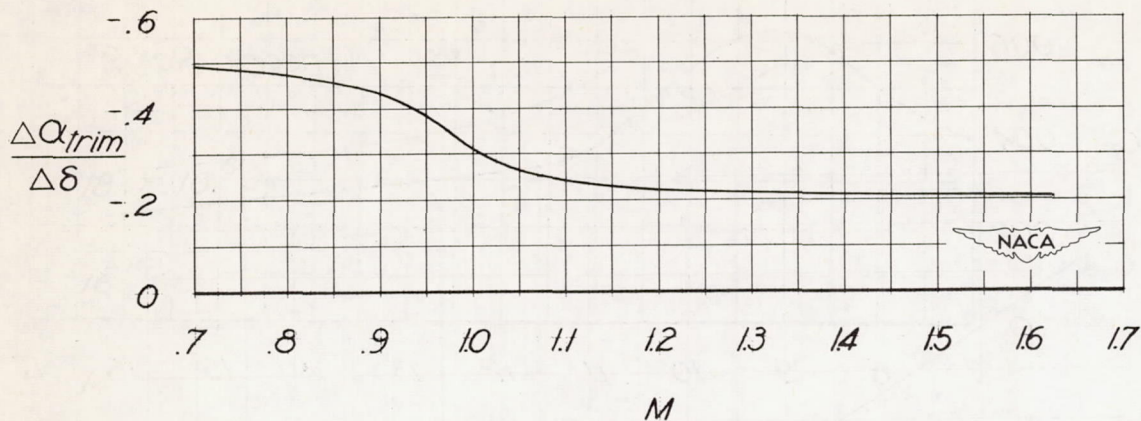


Figure 15.- Trim angle of attack produced by a unit control deflection.

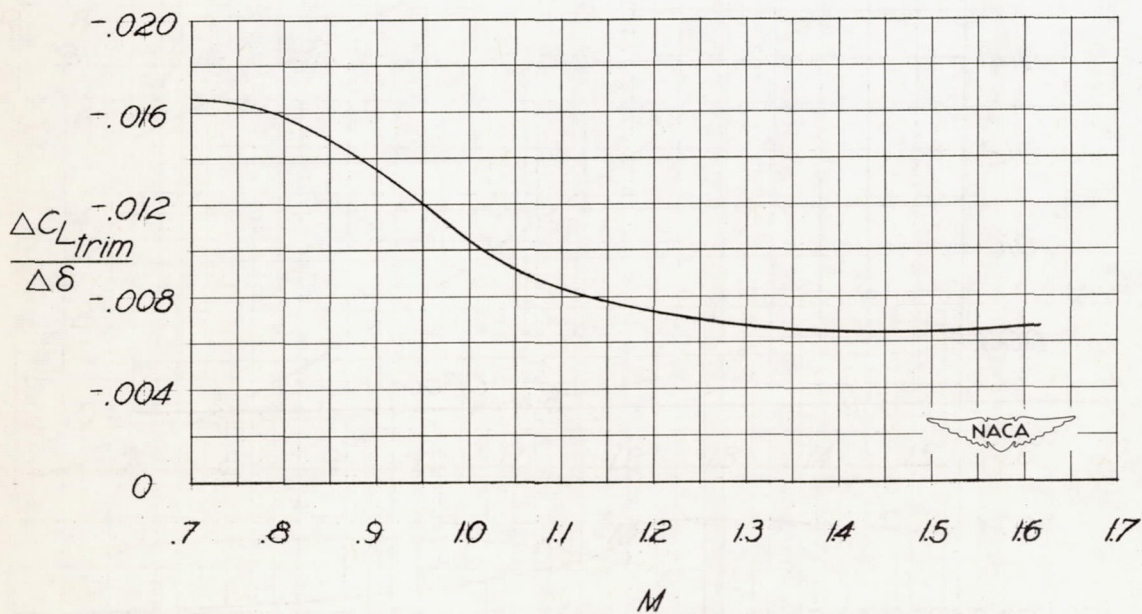


Figure 16.- Variation with Mach number of trim lift coefficient due to control deflection.

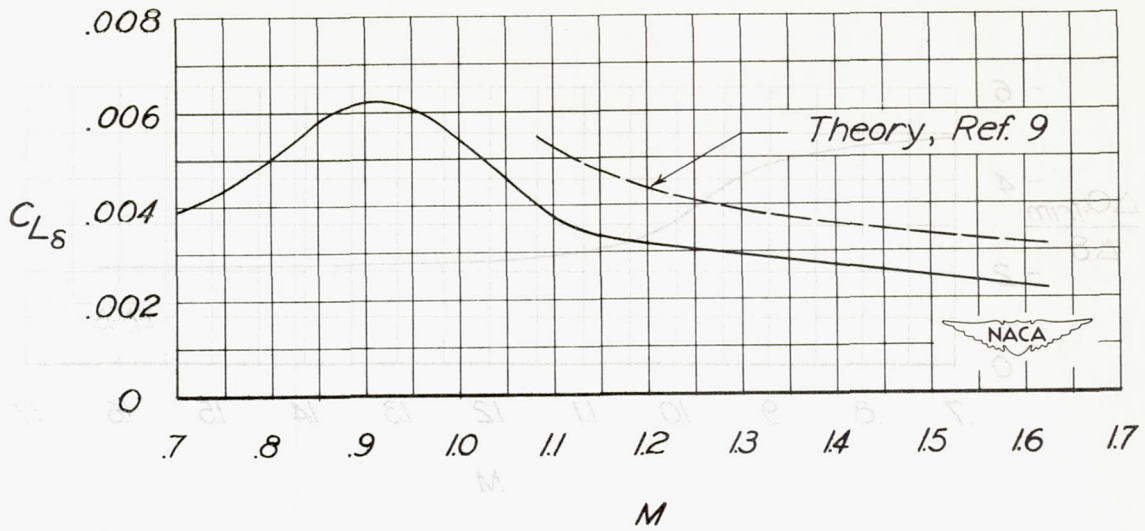


Figure 17.- Control-surface lifting effectiveness.

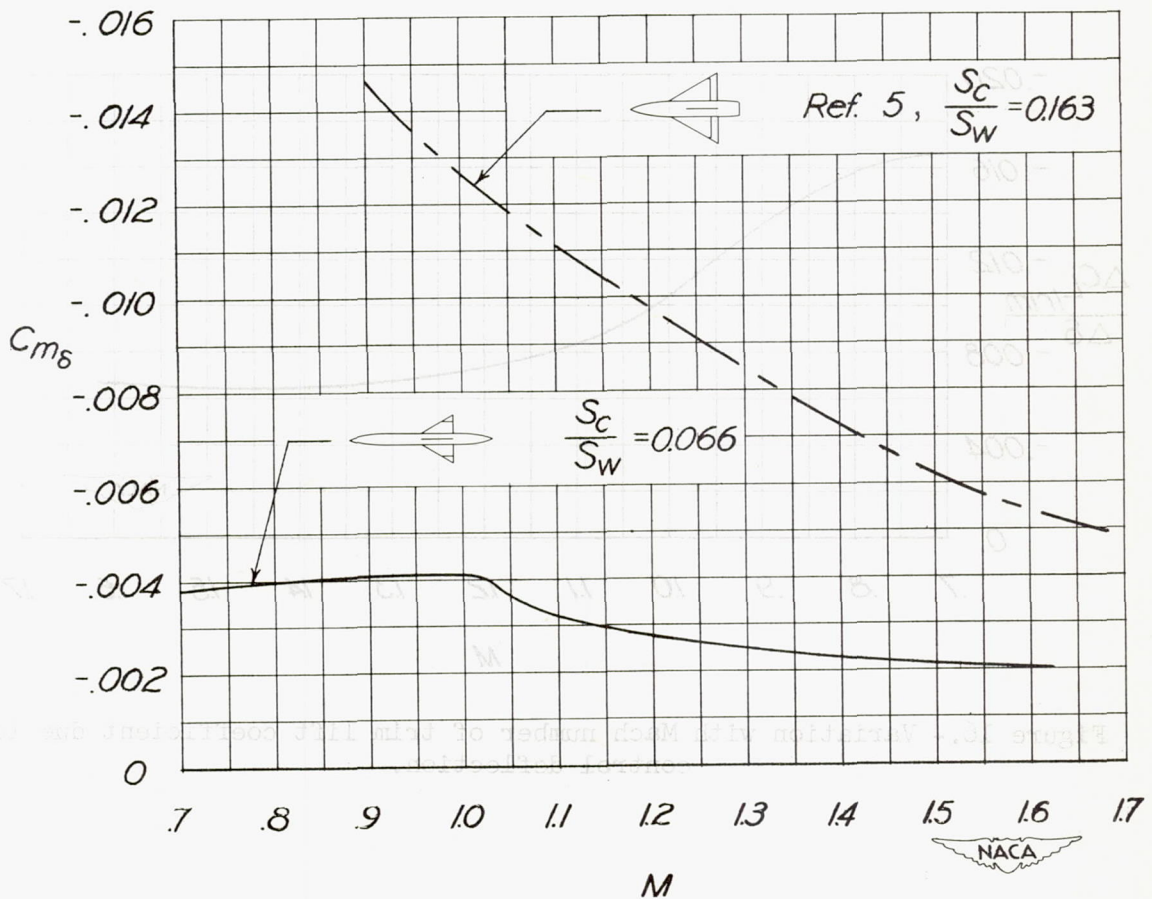


Figure 18.- Control-surface pitching effectiveness.

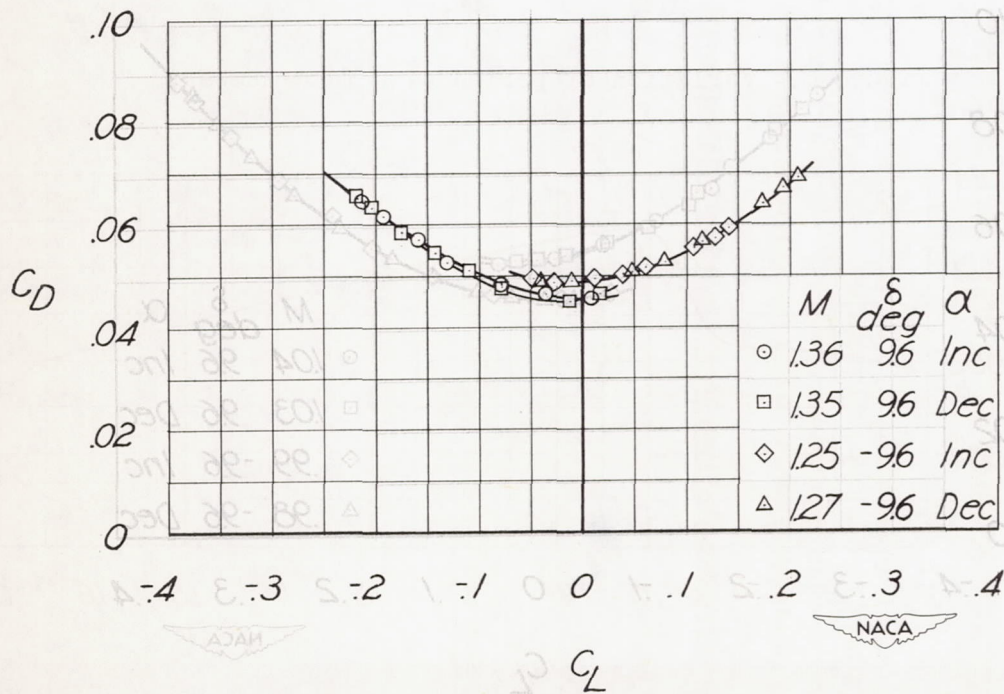
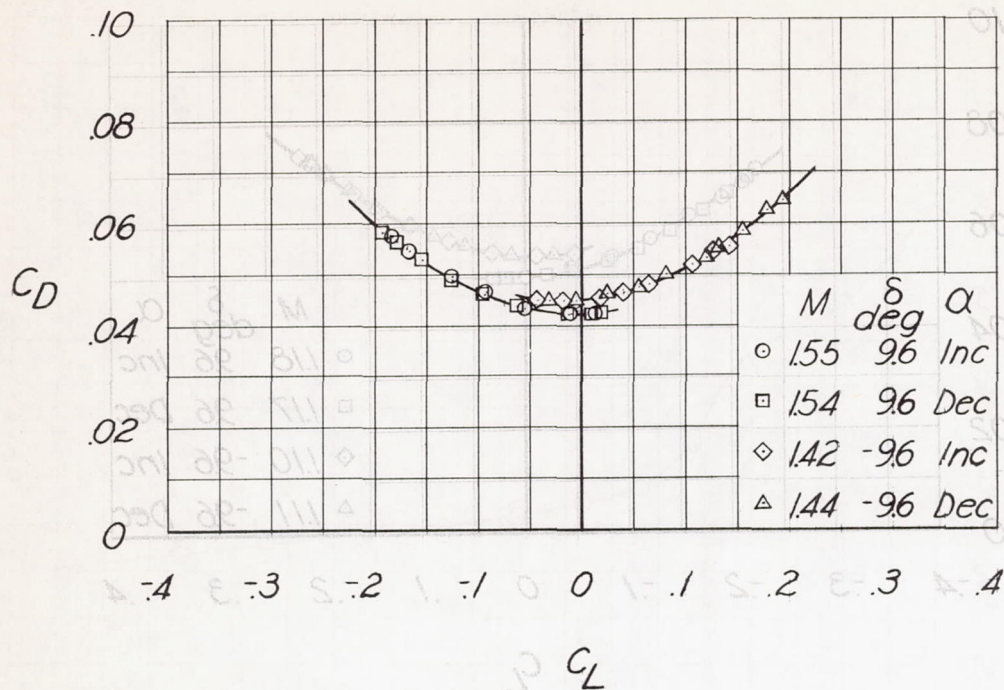


Figure 19.- Lift-drag polars.

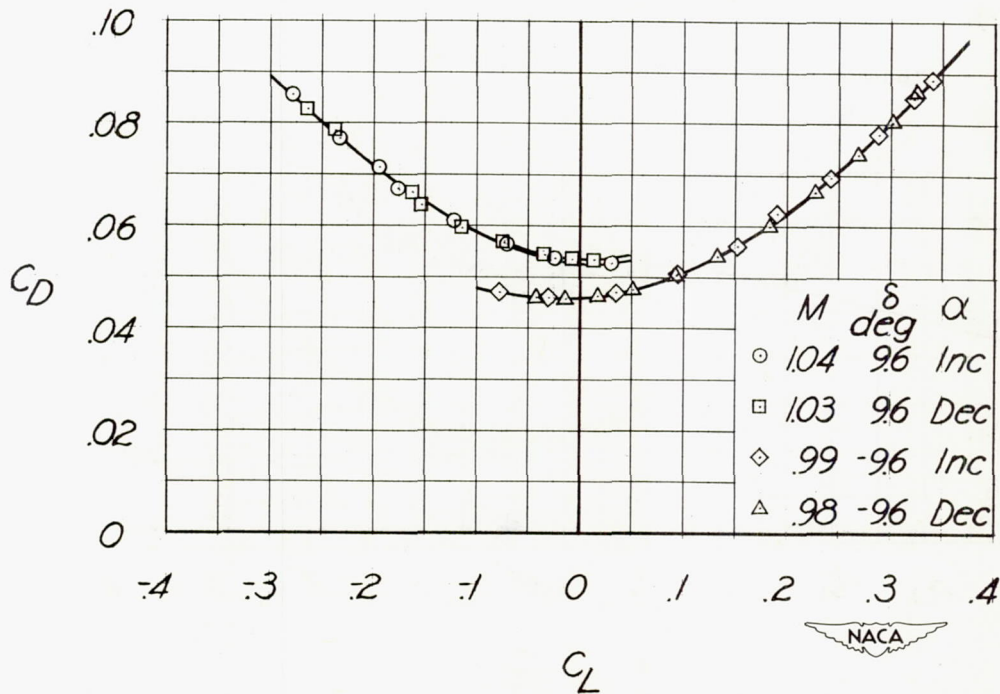
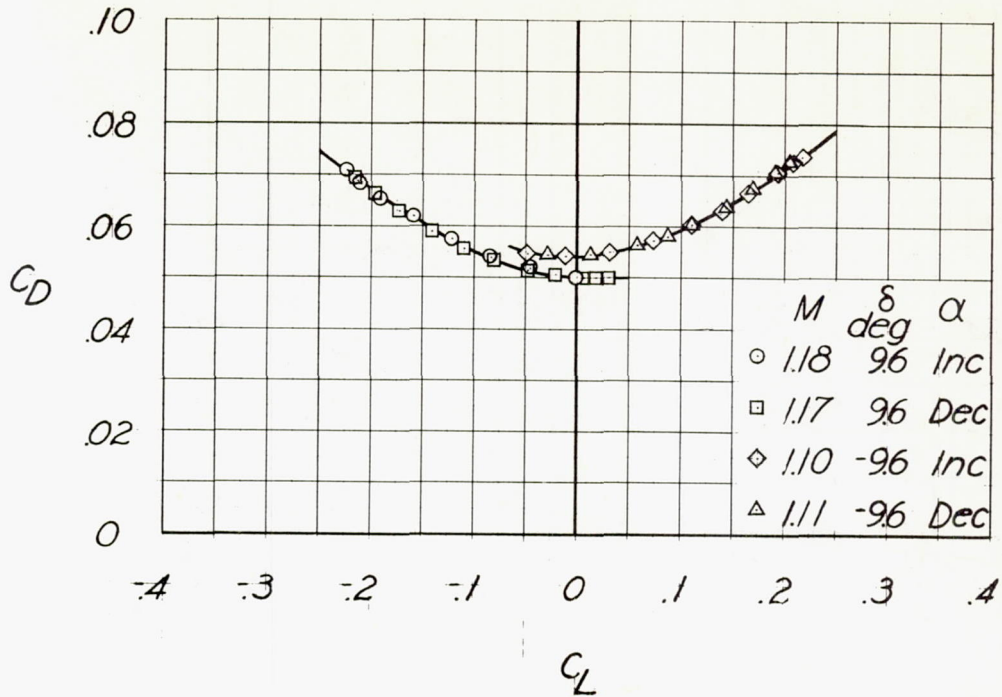


Figure 19.- Continued.

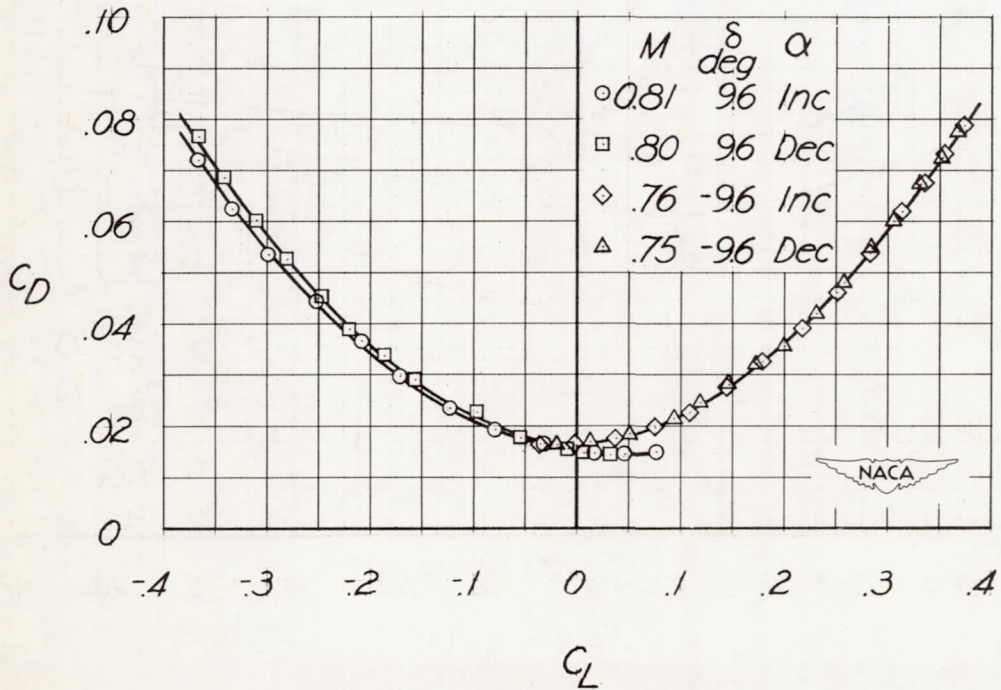
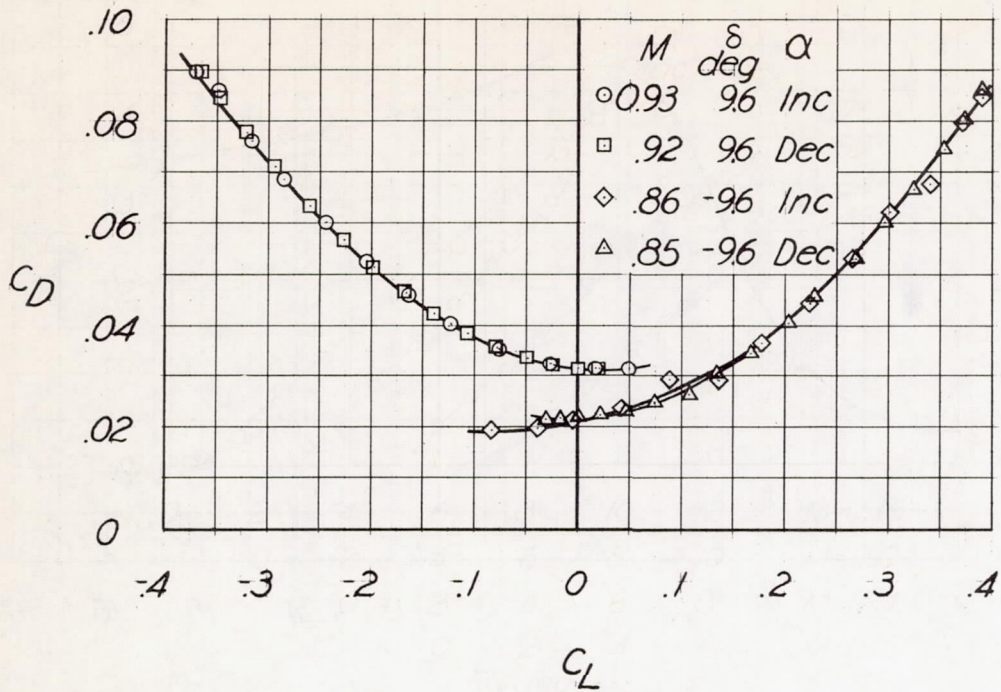


Figure 19.- Concluded.

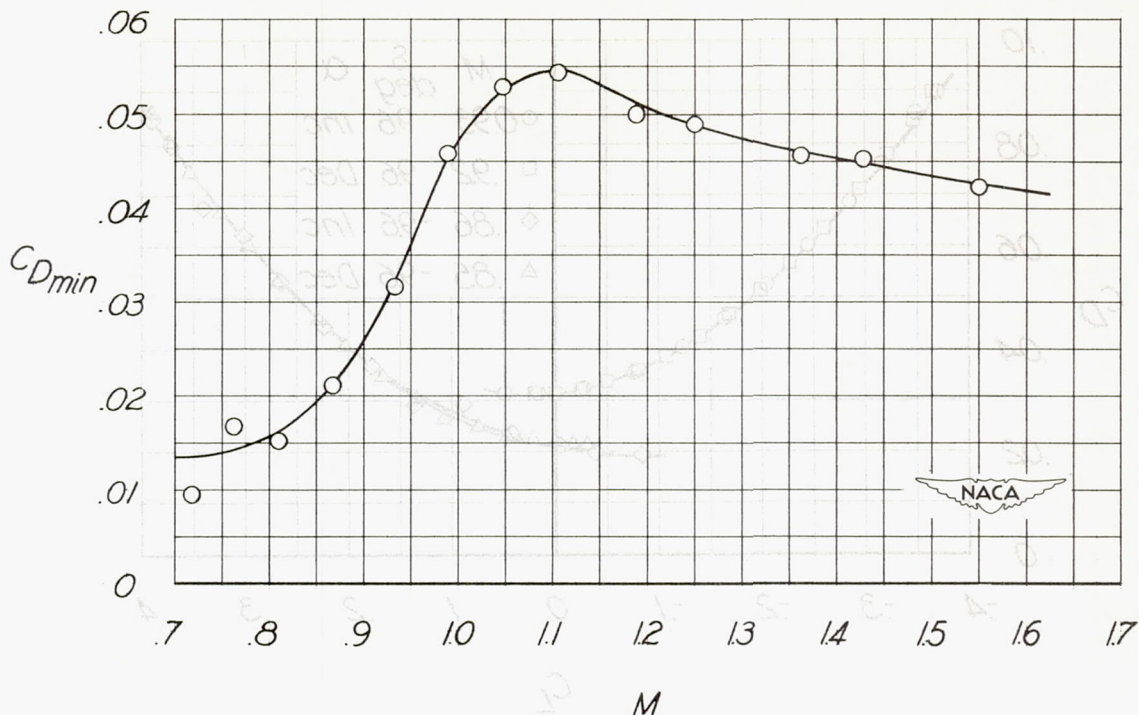


Figure 20.- Variation of minimum drag coefficient with Mach number.

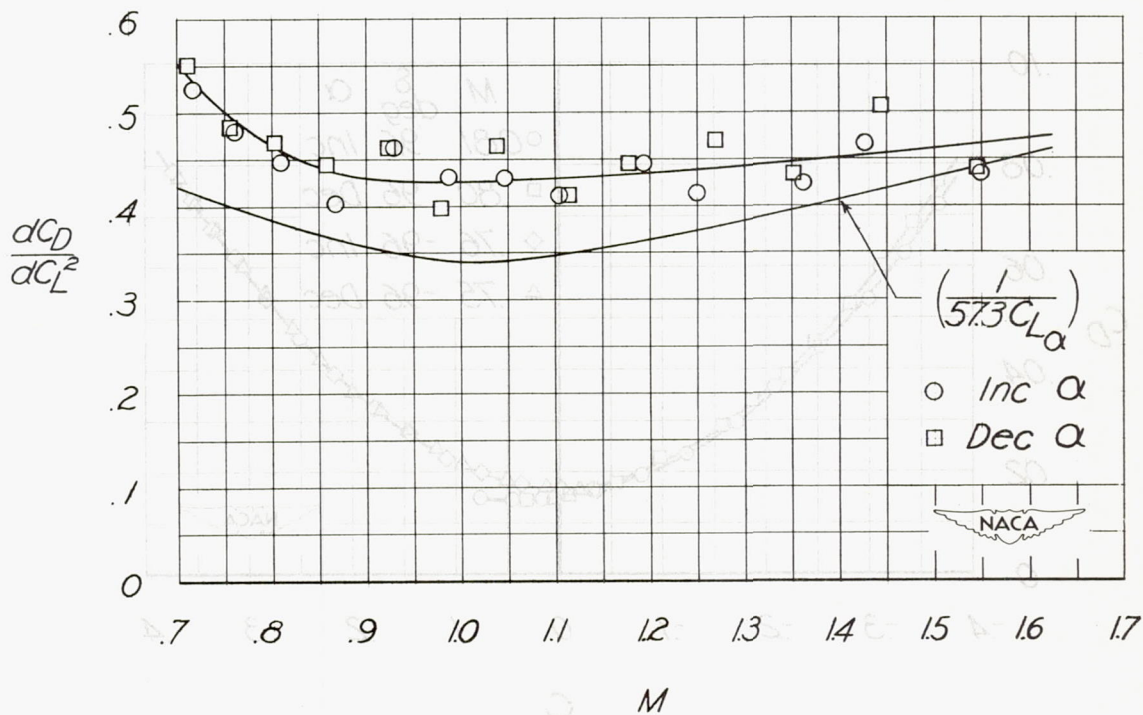


Figure 21.- Effect of lift on drag.

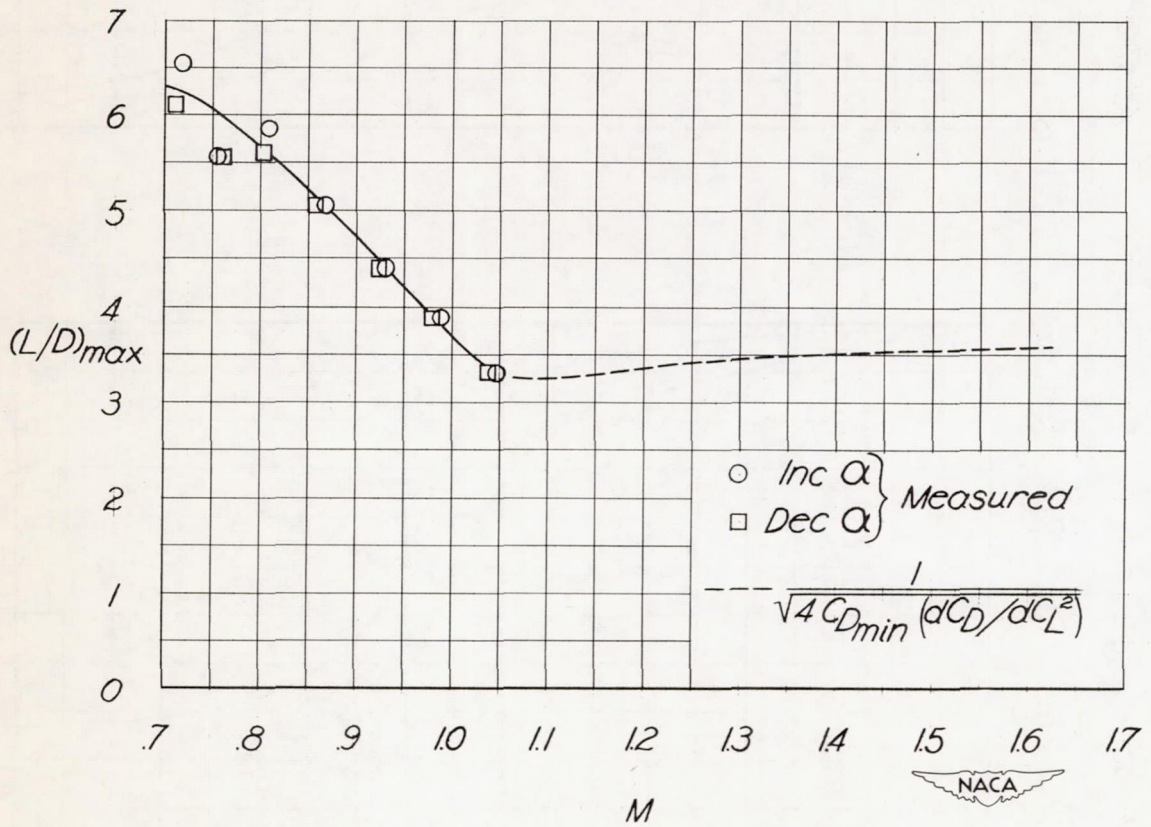
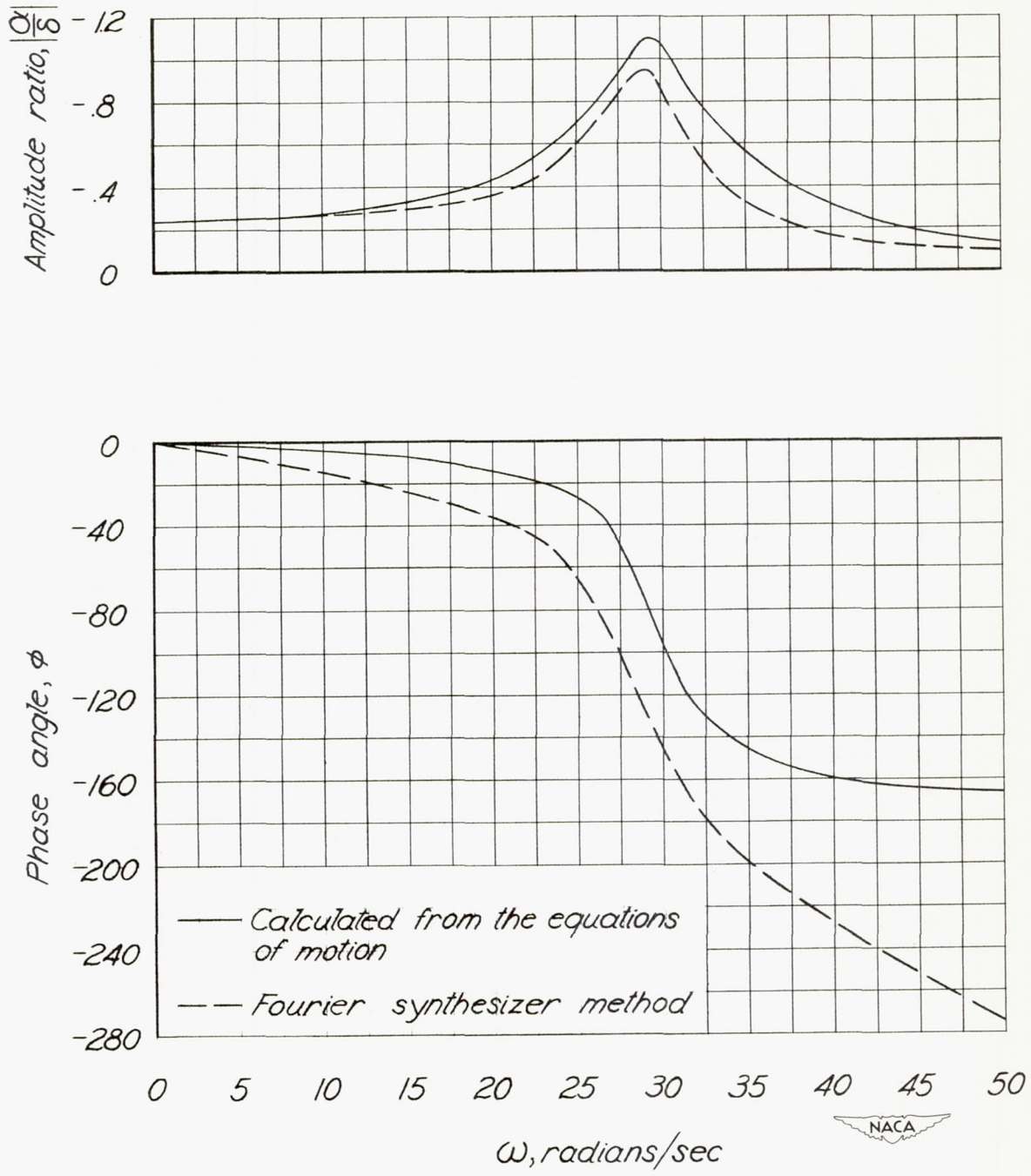
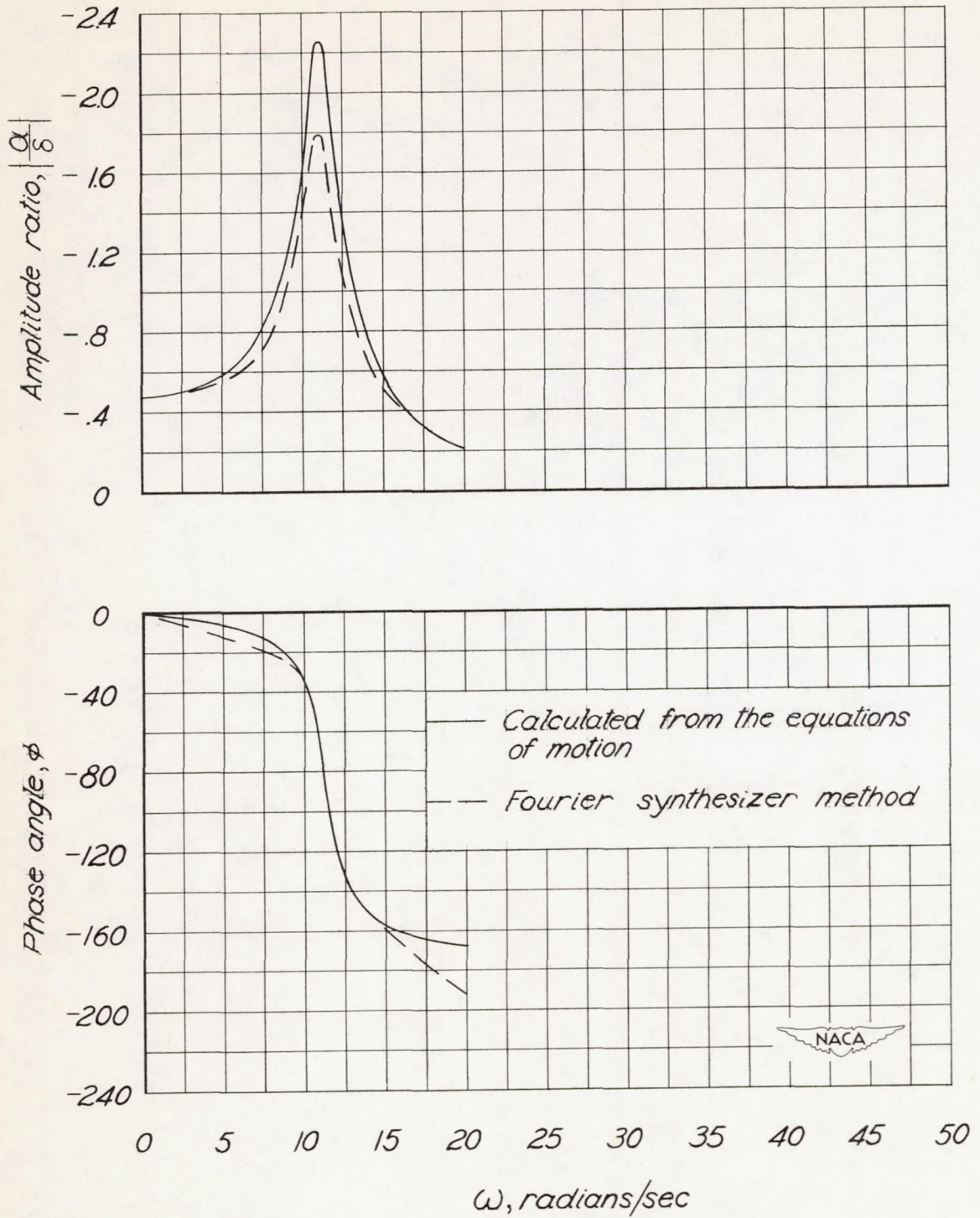


Figure 22.- Variation of maximum lift-drag ratio with Mach number.



(a)  $M = 1.60$ .

Figure 23.- Comparison of frequency-response methods.



(b)  $M = 0.74$ .

Figure 23.- Concluded.